Chapter 2

BACKGROUND

In the first section of this chapter first-year ridges are defined and the geometry and composition of ridge keels are investigated. The shear strength of ice rubble is reviewed from the open literature in Section 2.2. Forces resulting from ridge interactions with structures are described in Section 2.3 where laboratory and full-scale data are documented. Section 2.4 reviews the evolution of keel load models and looks at the performance of several models in a sensitivity analysis.

2.1 First-year ridge characteristics

2.1.1 Definitions and formation processes

According to the Canadian Code for Offshore Structure Design (CAN/CSA-S471-92) *first-year ice* is defined as "sea ice not more than one winter's growth". A *ridge* is defined as "an approximately linear ice feature of broken ice blocks, created by pressure due to relative motion, that can be categorized as a shear ridge or a compression ridge". A *compression ridge* is formed at the boundary of two ice sheets or spontaneously within an ice sheet as the result of excessive compressive stresses (Figure 2.1). A ridge formed in this way through the dynamic action of current and wind driving forces is often irregular in direction, height and depth. Compression ridges can be quite large with extreme sail heights 10 m or more and keel depths of 40 m or more (CSA-S471-92). Most first year ridges, however, have sail heights less than 6 m (Wright *et al.* 1978) in the Beaufort Sea and less than 2.5 m in the Northumberland Strait (Brown, 1989).

A *shear ridge* is formed by lateral movement between ice sheets and, in contrast to more common compression ridges, is straight and dense with near vertical walls. They do not arise spontaneously from level ice but rather result from the shear action between already separate ice sheets, at the interface between moving and landfast ice, or from compression ridges which have undergone a change in driving force direction. The distinction between shear and compression ridge keels is not made in this thesis.

Ridging occurs in most of the arctic and subarctic seas and estuaries and is also a common occurrence on larger freshwater lakes, for example, Lake Erie. Rubble *pile-up* and *ride-up* occur when floes are driven ashore or grounded leading to significant rubble mounds. Similarly, ice rubble *jams* are formed when passage of floes is obstructed and *bridging* occurs. *Rubble fields* may be formed when a pressure ridge grounds and sustained driving forces cause continued floe ice failure leading to the significant broadening of the rubble formation. This thesis is concerned with floating first-year ridges which in some circumstances may be laterally extensive making them indistinguishable from floating rubble fields.

The process of compression ridge formation is not well documented though it is thought to be fairly rapid - a matter of hours and minutes to form. It involves the crushing and fracture of the ice sheet into blocks and brash that are ultimately forced beneath the surface forming the keel and to a lesser extent are forced upwards to form the sail, thus maintaining hydrostatic equilibrium. The multi-failure mode process of formation may grade rubble and contrasts to other rubble formation mechanisms. At the Kemi-1 lighthouse in the Gulf of Bothnia level ice interacting with the lighthouse structure penetrated a stationary rubble pile and failed directly against the conical shield. The

rubble formed in this way was regular in shape and almost uniform in size (Hoikkanen, 1985). The thrusting and mixing action during ridge formation may be expected to sort blocks somewhat, with slush at the waterline and large blocks on the bottom of the keel and the top of sail. The same action may also rupture freeze-bonds between newly submerged cold blocks or cause rubble *clumps* to form.

In time, through heat transfer, pressure bonding, sintering and/or other processes, compression ridges may become partially *consolidated*, the term used to describe the freezing of pore water and the bonding of juxtaposed blocks. An irregular solid ice layer (referred to as a refrozen or consolidated core) which forms at the waterline within a ridge separates the keel from the sail and may exceed the parent ice layer thickness by two or three times (Eranti *et al.* 1992). This three-part ridge approximation is shown in Figure 2.1. Variations of this ridge representation are common in the literature. Eranti *et al.* (1992) prefer to separate the keel into two regions; an upper one comprised of heavily compacted and consolidated blocks, and a lower one comprised of loose and partially adfrozen blocks. Gladwell (1976) and others describe significant slush layers below the core, and Lepparanta *et al.* (1995) document a distinct mid-keel low porosity region. Most field studies indicate that ridge structure is likely to vary spatially and temporally. Keel form is probably influenced by formation temperature and speed, parent ice salinity and thickness, ridge depth, sail size, the elapsed air and current exposure, and local snow regime. Ridges which survive the first melt season as second-year and multi-year ice features consolidate further, reducing porosity and increasing strength to become formidable obstacles to any structure. Second-year and multi-year ridges occur mostly in arctic regions and are not considered in this thesis.

2.1.2 Parent ice properties

Detailed information on the physics of ice is found in Pounder (1965), Hobbs (1974) and Michel (1978). Cammaert and Muggeridge (1988) and Sanderson (1988) document investigations of ice properties and ice interactions with offshore structures. A review of the mechanical properties and formation processes of sea ice, the constituent material of ridges, was carried out as part of the work for this thesis and published in Bruneau (1995a). Sea ice formation processes, morphologic and strain rate characteristics and strength and friction properties were documented in that study. Table 2.1 summarizes some of these first-year ridge parent ice properties for reference later in the text.

2.1.3 First-year ridge geometry

Several researchers (Weeks and Kovacs, 1970, Wright and McGonigal, 1982, Kankaanpaa, 1989) have documented the geometry of first-year ridges in detail. Others (Acres 1987, Cammaert *et al.*, 1993, Croasdale *et al.*, 1995, Burden and Timco, 1995) have sought to classify ridge geometries for interpretive or design purposes. A summary of first-year ridge characteristics from the literature is presented in Table 2.2, and significant keel parameters are reviewed below.

Keel size and shape

Dolgopolov *et al.* (1975) describe the geometry of first-year ridges in temperate regions around Russia. They observed that the design ratio of ridge draft to depth may be taken as 1/4 to 1/5 and that an individual ridge may have a trapezoidal cross-section. Kankaanpaa (1989) in a survey of 8 ridges in the Baltic Sea found the sail height to keel depth ratio was 1/5.8 on average though it ranged from 1/3.8 to 1/8.6 and local isostatic imbalance was common. In another Baltic study this ratio ranged from 1/4 to 1/8 (Veitch

et al., 1991a). Burden and Timco (1995) produced a catalogue of sea ice ridge morphology in which one hundred and seventy-six multi-year and first-year ridge profiles from the literature are documented. The keel depth to sail height ratio for first-year ridges in temperate regions was found to be 3.96, almost identical to that of keel width to depth, 3.94. Considerable scatter was observed in the data and it was noted that the power law fit, $W = 5.76H^{0.86}$ (where H is keel depth and W is keel width) may be more appropriate than the linear model. Note that the keel depth, H, is usually measured from the waterline. When considering ridge force models, keel depth is typically reduced by the thickness of the submerged portion of the refrozen core (Cammaert *et al.* 1993).

Kankaanpaa (1989) found average slope angles of the sail to be 21° and keel slopes to be around 32°. Cammaert and Muggeridge (1988) report that a typical first year ridge keel has a mean keel angle of 32°. This implies that a keel width to depth ratio of 3.2 can be expected for triangular-sectioned ridge keels. Lepparanta and Hakala (1992) note that in the six ridges they studied they found the largest maintained a well developed triangular cross section (depth of 14 m) whereas the medium-sized (depth approximately 5 m) were more trapezoidal. Smaller ridges lost the appearance of being identified as a ridge as the keel was more closely described by an irregular rubble field. Lepparanta *et al.* (1995) suggest that ridge keels may start out triangular in shape but evolve towards a trapezoidal form. The *keel angle* defined by Burden and Timco as "the angle of decline for each side of the keel in degrees" for 35 temperate region ridges had a mean of 27.6° and a standard deviation of 13.9°, suggesting considerable variation.

Apparently, the limiting vertical size of ridge sail height (H_s) depends upon the thickness of the parent ice sheet, h. The relation to keel width and depth is thus implied from

ratios given above and in Table 2.2. Lepparanta and Hakala (1992) present the formula as

$$H_s = Ch^b \quad (1)$$

where C and b are constants. Parmerter and Coon (1972), Lepparanta (1981), Tucker *et al.* (1984) and Timco and Sayed (1986) obtained different values for b, typically between 0.5 and 1. Kankaanpaa (1989) determined that the best positive correlation occurred when $C = 2.2$ and $b = 0.5$. Many statistical aspects of arctic ridge height, depth and spacing are considered by Hibler *et al.* (1972). They found remarkably good characterization of ridging using just the ridge height and ridge spacing within a floe, and also found a linear relationship between those parameters.

Keel porosity

The porosity of ridge sails and keels has been studied by several researchers (Kovacs and Mellor, 1974, Keinonen, 1977, Tucker *et al.*, 1984, Kankaanpaa, 1989, and Lepparanta and Hakala, 1992). Some results are listed in Table 2.2. Keel porosity is usually determined by mapping the resistance felt while drilling a vertical hole through a keel. In Baltic research it is common to categorize resistance into regions of slush, solid ice, no ice and loose blocks. Other sources from elsewhere cite void ratio only. Careful excavation and block measurement in the sail (Veitch *et al.*, 1991b) have also provided insight into ridge porosity by an assumed equivalence or through buoyancy equilibrium calculations. Since interpretive techniques vary and significant spatial and temporal variability is expected, porosity measurements in most respects are approximate.

Field drilling results in the Baltic indicate that the average porosity for a whole ridge is

29% but varies with a standard deviation of around 4-6%. Keel porosity is typically larger than sail porosity (8% more according to Kankaanpaa, 1989). According to Lepparanta and Hakala (1992) there is little explanation for this but that block size distributions may vary - this is as yet unproven. Eranti *et al.* (1992) describe a layering in the ridge keel but this is more a boundary between a region of heavily and loosely packed blocks at around 1/3 of the ridge depth. Lepparanta *et al.* (1995) describe porosity layering (minimum at mid-keel range) and evolution though results are based on a single ridge. Note that the maximum packing density of uniform spheres gives a porosity of 25%, which is quite close to the rubble values.

Ice block size, shape and placement

Weeks and Kovacs (1970) investigated first-year ridge keels near Barrow Alaska. Results from one ridge indicated that the keel was comprised of two different parent ice thicknesses: 15 to 20 cm and 50 to 60 cm. The coring of the keel showed a heterogeneous layering of sea ice and snow and slush ice that was poorly bonded. Larger blocks on the outer edge of the keel were rounded indicating appreciable melting. Other ridges had parent ice thicknesses of the order of 15 to 20 cm.

The piece size distribution of ice blocks in the sails of Baltic sea ridges has been investigated by Veitch *et al.* (1991a, 1991b). In two separate studies it was found that the sample distribution for both long and short ice block axis was near lognormal, and was thus represented by

$$f(x) = \frac{1}{x\sqrt{2\pi}\ln x_{sd}} \exp\left[-\frac{1}{2}\left(\frac{\ln x - \ln x_m}{\ln x_{sd}}\right)^2\right], \quad 0 \leq x < \infty \qquad (2)$$

where x_m is the geometric mean and x_{sd} the geometric standard deviation of the distributed quantity x. In one study of two ridges in the same vicinity Veitch *et al.* (1991a) determined that the mean block long axis lengths were 55 cm and 49 cm and the mean short axis lengths were 36 cm and 34 cm respectively for the two ridges. The long axis standard deviations were 2.2 and 1.7 cm. The long-to-short axis ratio for the two were 1.52 and 1.49 with a mean thickness recorded at 0.18 m and 0.19 m respectively. Over one hundred ice blocks were measured in that study. In another ridge study located elsewhere in the Baltic, Veitch (1991b) found that the mean thickness, long axis and short axis dimensions for two different locations in a ridge sail were 16 cm, 71.2 cm and 69 cm, and 15 cm, 54 cm and 50 cm respectively. Distribution lognormality was again established.

Lepparanta and Hakala (1992) studied 6 ridges in the Baltic and found the average thickness of ice blocks to be around 10-30 cm and the average length to be 60-90 cm. They determined that the block size distribution was quite narrow, the maximum lengths being less than twice the average length. The ice blocks in the keel were characterized as platy, well-rounded and often very porous. The blocks also appeared to be randomly arranged and the existence of the occasional very large block (some ten times bigger than the average in length) situated in the middle or near the bottom of the keel, was noted.

2.1.4 Temporal ridge keel processes

Evidence that ridges undergo considerable changes through a season is provided by the research of Peschansky (1963), Weeks and Kovacs (1970) Lepparanta *et al.* (1995) and others. Mechanical and thermodynamic processes result in erosion, re-packing, creep, melting, freezing, brine ejection and recrystallization. How these and other processes

interact is not known but by the following description the changes are significant (from Lepparanta *et al.* (1995) describing the life-cycle of a Baltic first-year ridge):

> "The ridge structure underwent considerable evolution. The external geometry became smoother. The keel depth and sail height decreased and the cross-section developed from triangular toward trapezoidal form. The volume of the ridge showed no significant changes in the mid-winter but decreased by 25% during one spring month. The porosity of the ridge decreased from 28 to 18%; it varied vertically through the keel and showed a persistent minimum of 20 to 23% in the mid-keel region. The decrease was in midwinter and was due to further consolidation and packing of ice blocks while in spring packing compensated the porosity increase by melting for the mid-range data. During the melting season, below the consolidated layer the melting of the ice blocks was found to be uniform and the same as the overall ice volume decrease; mechanical erosion of the keel was insignificant."

Practically no information is available on ice block erosion and other mechanical "aging" processes. Since this is not the intended focus of research for this thesis the topics are not discussed further, however, they may be important and should be considered in future research efforts. Keel consolidation, block bonding and creep are reviewed below to provide some background for a discussion later on rubble shear strength.

Refrozen core formation

Depending on the air temperature when compression ridges form, the parent ice may often be a few degrees cooler than freezing (according to the air temperature). The

negative sensible heat of ice blocks in the keel must then be considered for both the potential contribution to the growth of the refrozen layer and in the freeze-bonding of ice blocks. Lepparanta and Hakala (1992) illustrate this capacity in the following example. Consider a rubble layer of thickness, H, porosity e and temperature T. This layer may produce in water a surface ice layer of thickness h' which is obtained from

$$\rho_i L h' = \rho_i c_i (T_f - T)(1-e)H \qquad (3)$$

where c_i is the specific heat of ice, L is the latent heat of fusion and T_f is the freezing point temperature. If $T_f - T = 5°$ and $H = 5$ m, then $h' = 10$ cm. Further, the decrease in porosity that may be expected as a result of the cold content of the blocks being used up in freeze bonding alone would be 3% if the ice block temperature were 5 degrees below freezing upon formation.

The long-term growth of a refrozen core in a ridge is predominantly attributed to heat conduction to the cold atmosphere. Stefan's model for level ice growth is often used to predict this growth. It is commonly represented as

$$h'^2 = \frac{2k}{\rho_i L}\int_{t_o}^{t_f}(T_f - T_i)dt \qquad (4)$$

where T_f and T_i are the freezing temperature and ice surface temperature respectively, and the constants k, L and ρ_i are the mean thermal conductivity, latent heat, and density of ice. The time t_o is the time at which the ice begins to form. In a ridge or rubble field only the water in the voids of the rubble must be frozen for the increase of vertical core ice thickness. Given that the square of the ice thickness is inversely proportional to ice density and latent heat (typically around 333 J/g) and directly proportional to thermal conductivity (approximately 2 W/m °C) it is evident that the square of the thickness

should also be inversely proportional to the rubble porosity. This hypothesis was tested by Veitch *et al.* (1991c) in a laboratory experiment in which ridges were produced under controlled conditions and the degree of ice growth was measured. It was determined that core ice grew at a rate of 1.8 that of level ice when rubble porosity, e, averaged 39.5%. The predicted growth based on the $e^{1/2}$ ratio suggests a ratio of 1.6, a reasonable agreement given that the conditions under which these tests were conducted were somewhat ideal (little temperature variation, and with natural insulation from snow and ice not modelled).

Croasdale, Allyn and Marcellus (1990) devised a comprehensive computer model for predicting the refreezing of ice rubble. Their model considers air temperature, wind speed, radiation, ice temperature, rubble porosity, rubble height, snow cover, salinities and other significant parameters. Their results indicated that the parameter which has the biggest degree of uncertainty and which is most important, is the initial porosity of the ice rubble. It is suggested that this parameter could vary with the initial effective stress state in the rubble due to sintering and creep consolidation, emphasizing the need for a better understanding of the state of ice rubble when it first forms and prior to refreezing.

In the design load calculation for the NSCP bridge (Cammaert *et al.* 1993) a model was developed from work by Nakawo and Sinha that considered the measured temperature regimes, ice thickness and snow deposition regimes in, and around, the Northumberland Strait. It was assumed that the region of the keel that undergoes consolidation had a porosity of 30% but that the pores were completely filled with brash ice and snow with a porosity of 50%, thereby reducing the porosity for freezing purposes to 15%. This assumption was precautionary and is expected to produce an upper bound for refrozen

ice layer growth.

It is generally accepted that the refrozen core thickness varies considerably over short distances. This variation is in part the result of randomly oriented blocks being partially incorporated into the core layer but is also due to non-uniform insulation above. Near the highest part of the sail (which often acts as a snow fence) the consolidated ice thickness is generally thinner than in most other areas above the keel. This would lead to the weakening of the level ice in this area which may influence ridge failure mechanisms. Most modelling strategies assume the core is a uniform thickened plate.

Keel block bonding

Some examinations of keel ice rubble *in situ* have been reported in the literature (Pilkington *et al.*, 1982, Shinde and Kemp, 1983, Brown, 1989, Lepparanta and Hakala, 1992, Eranti *et al.*, 1992 and others). Most describe rubble in the keel as highly variable in texture and geometry. Blocks may vary from porous and highly deteriorated to apparently solid plates (Weeks and Kovacs, 1970). Observations are typically limited though by lack of access to the outer surface of keels. Inter-block contacts are usually coherent ice bridges but are often weak enough that blocks may be dislodged by hand. In the Beaufort, Shinde and Kemp (1983) reported contact lengths less than 10% of block length in mature first-year ridges in April. The ice blocks were very easy to dislodge indicating that "the cohesive strength of the contact was less than 35 kPa (judged by comparison with observations with cohesive clays)". The crystallographic examination indicated that the frozen junction between blocks was comprised of relatively course granular congealed frazil ice. Ice blocks in the keel ranged from 0.3 to 1.8 m thick with lengths from 0.6 to 3.0 m and widths typically around one-half the length.

Inter-block freeze-bonding below the consolidated core may arise as a result of several processes. As mentioned previously the negative sensible heat in the blocks at the time of ridge formation may be converted to latent heat at block surfaces by (or during) fusion. Bonding by heat conduction may reach below the consolidated core through partially incorporated blocks or highly saline pore fluid. However, temperatures throughout the keel are usually at, or very near, the block melting point (Lepparanta *et al.*, 1995, Weeks and Kovacs, 1970, and others) so that this mechanism is probably not predominant. It is more likely that bonds result from *pressure consolidation*, *sintering* and other recrystallization processes which are briefly described below.

The freeze bonding that occurs between two ice pieces brought together was first described by Faraday in 1859. In the paper "On Regelations and the Conservation of Force" Faraday demonstrated that if two ice blocks are placed in contact they will form a solid bond even when the temperature of the ice and surroundings is such as to keep them in a thawing state. To explain this Faraday postulated the existence of a liquid-like layer on the ice surface which, when enclosed by ice at the point of contact, freezes. Disputing this, Thompson in 1857 argued that the minute areas over which the asperities on the ice surfaces contact one another were sufficiently small to create contact pressures which lower the equilibrium melting point. The melting which results then relieves the pressure which in turn causes the water to re-freeze and bond the pieces together (pressure consolidation). It is currently believed that the driving mechanism for bond growth between two ice pieces is an unstable thermodynamic system in that the surface free energy is not minimized. The energy of the system can be reduced if material is transferred to the region of contact thereby causing the bridge to develop (sintering). Although this theory is broadly accepted today, the mechanism by which the initial neck

forms between the two ice particles still remains uncertain.

Schaefer and Ettema (1986) carried out experiments investigating pressure consolidation/sintering between two flat surfaces of uniform freshwater ice blocks. Apparently, much stronger (greater than four times) freeze bonds develop between fresh ice blocks when immersed in fresh water than when in air, unless the water is a saline solution. In a saline solution (salts greater than 12.5% by weight) bonding is weaker than that in air. The strength of the freeze-bond between blocks in fresh water increased linearly with increased normal pressure and duration of contact. However, in saline solutions (salts 3% or greater) the increase with normal pressure is much weaker and no bond strength increase was observed for increased contact durations. Schaefer and Ettema concluded:

- Stronger freeze bonds form in water than in air (submerged rubble will have a pronounced cohesive character, and associated with this is a pronounced effect of loading rate in which strength decreases with increased rate).

- Cohesion in a floating rubble ice layer probably increases with increasing depth due to higher normal pressures.

- Contributing to the scatter of data from rubble shear strength tests in the literature is the time between experiments since stronger freeze bonds form with increased duration.

Bulk pressures in ridge keels are usually determined by the product of rubble buoyant

weight and position above the keel bottom, z, as follows:

$$\sigma_v = (\rho_w - \rho_i)(1-e)gz \qquad (5)$$

where ρ_w and ρ_i are the densities of the water and ice, σ_v is the bulk vertical stress in the rubble, e is the bulk porosity of the rubble, and g is the gravitational acceleration. Initially first-year ice blocks may have densities ranging from 860 to 920 kg/m^3 (σ_v changes by a factor of two in this range). In time, though, all submerged rubble probably has a density greater than pure ice (917 kg/m^3) since evacuated brine channels are likely to fill with water (anomalously, the "heaviest" blocks may become the "lightest"). For example, maximum bulk pressures for a 20 m deep keel of porosity 30%, and block density of 900 kg/m^3 in sea water of density 1028 kg/m^3 are around 17.6 kPa. Pressures between blocks are, of course, much higher. If contacts were 10% of block length as described by Shinde and Kemp (1983), then notionally contact areas may be 1% of total so that pressures would be 1.76 MPa. This pressure exceeds the crushing strength of warm unconfined sea ice and so contact areas would grow. This example is probably overly-simplistic, but it serves to illustrate the stress level which may lead to pressure bonding.

Pressure consolidation and sintering may be important bonding mechanisms but other complicated processes may also be at work. Circulation is likely to be important for redistribution of brine and or frazil ice. Lewis and Perkin (1986) describe the phenomenon of an *ice pump* which is a naturally occurring heat engine driven by the change of freezing point with pressure. It causes ice to melt at lower depths in sea water and to form at a shallower location - and is a self-starting mechanism. The pumping is not dependent upon the availability of sensible heat in the water column and its effects

are added to any melting caused by the advection of warmer water to the ice-water interface. It is conjectured that, due to the significant ice surface area in an ice rubble keel, level ice growth and keel deterioration may be enhanced appreciably via the *ice pump* mechanism.

Creep

Though ice deforms in several ways under pressure (as described in Table 2.1) irreversible secondary creep (viscous) strain is the most likely mechanism for causing noticeable global deformations in ridge keels. Blocks juxtaposed and under high contact pressure will deflect and contact areas will grow as ice "flows" in accordance with grain size, grain orientation, stress patterns and salinity. Sea ice containing brine flows more easily than pure ice since brine cannot support shear stress. Pockets of brine also cause stress concentrations which further enhance creep rate. Though bulk rubble has a relatively low buoyant weight it was shown earlier that stresses between blocks in a keel can be high. Edge-on contacts between blocks may have contact areas defined by the compressive strength of the ice. Furthermore, the action of leverage from eccentrically applied buoyancy forces on blocks may promote near-failure stresses within blocks or at inter-block bonds. At 1 MPa the uniaxial strain rate for horizontal compression may be between 10^{-6} s^{-1} and 10^{-4} s^{-1} (Sanderson 1988) suggesting the potential for large deformations during the typical life expectancy of a ridge (around 100 days or $10^{6.94}$ s).

Table 2.1 Typical first-year ridge parent ice characteristics.

Ice type	Vertical Columnar S2 resulting from preferential growth perpendicular to 'c' axis.
Ice salinity	5-12 ppt brine in ice when sea ice comprised of 35 ppt dissolved salts.
Freezing point	-1.91 C at 35 ppt ; -1.1 C at 20 ppt ; - 0.3 C at 5 ppt
Ice density	860-920 kg/m^3 first-year sea ice ; 916.8 kg/m^3 fresh water ice
Sea water density	1028 for S = 35 ppt, T = -1.8C, 1016 for S = 20 ppt, T = -1.1 C
Ice friction	Dynamic ice-ice = 0.016-0.13 for -19 C to -5 C and from 0.06 to 0.83 m/s.
	Static sea ice-steel = 0.3-0.7 ; kinetic sea ice-steel = 0.025-0.25
	Sea ice-aluminum: static increases 4 orders from -1 C to -25 C.
	Sea ice-aluminum: dynamic decreases 1 order when speed rises 0.3 to 5 m/s.
Ice friction causes	Adhesion at contact asperities where weld-bonds form from high pressure.
	Liquid layer from loose surface molecules, pressure melting or surface friction may lubricate. Water vapour and surfaces gases also decrease friction.
Ice frictrion notes	Sea ice has higher friction coefficient than pure ice. At high normal loads
	friction coeficients decrease with increased pressure, esp. near freezing point.
Latent heat of fusion	264 J/g for ice salinity 8 ppt, temp = -2 C
	334 J/g for ice salinity 0 ppt, temp = 0 C
Thermal conductivity	2.13 W/(m C) for ice salinity 4.7 ppt, temp = -5 C
	2.22 W/(m C) for ice salinity 0 ppt, temp = 0 C
Specific heat	7.97 J/(g C) for ice salinity 10 ppt, temp -5.6 C
	3.25 J/(g C) for ice salinity 2 ppt, temp -5.6 C
Elastic modulus	Sea ice modulus varies with temperature and air plus brine volume.
	Dynamic values typically range between 3.5-9.4 GPa.
Morphology	Visco-elastic crystaline near melting point as when submerged.
Strain types (figure below)	Ductile, transitional, brittle.
Strain factors	Load rate, load concentration, load history, temperature,ice purity, porosity.
Ductile strain	For tension and compression: strain is immediate elastic then transient,
	delayed elastic, followed by time-dependant, non-linear viscous creep.
Brittle strain	Vacancy diffusion and dislocation velocities are too slow for ductility.
Ice strength - brittle	Governed by grain size, and brine volume. It is not as rate sensitive as ductile.
Compressive strength	Usually determined by uniaxual compression tests.
	May vary inversely with log of contact area.
	Typical measurements in lab between 1and 10 MPa, for larger scale < 1 MPa.
	Confinement suppresses crack propogation and enhances creep.
Tensile strength	Determined with direct tension tests.
	Influenced by salinity and temperature.
	Same order but slightly less than pressure strength values for compression.
Shear strength	Shown to vary with brine volume - wide range reported in literature.
	0.5 MPa aproximate average.
Flexural strength	Function of brine volume (salinity and temperature dependent).
	Usually lies between 0.1 and 1.0 MPa.
References:	**Sanderson (1988), Hobbs (1971), Pounder, (1968), Cammaert and Muggeridge (1988), Molgaard and Jordaan (1994)**

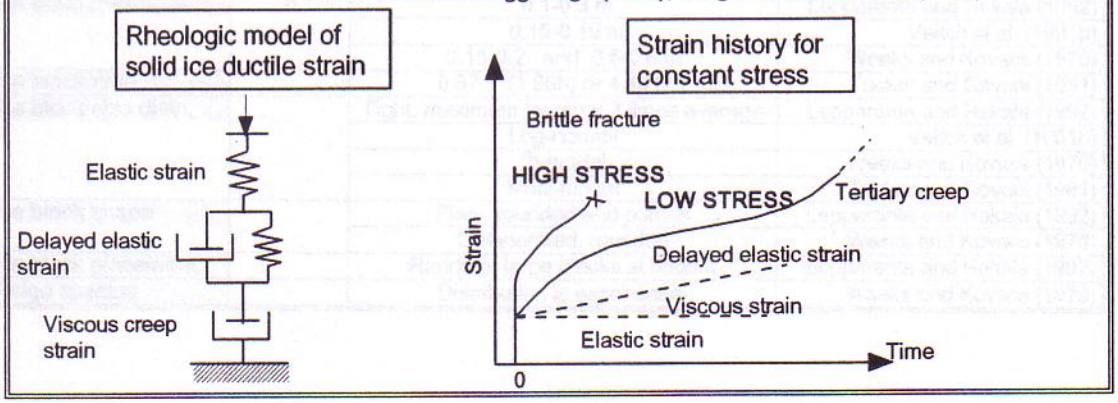

Table 2.2 First-year ridge characteristics reported in the literature.

Property	Symbol	Description	References
Keel width	*W*	3.94H or 5.76 H^0.86	Burden and Timco (1995)
		3.2H	Cammaert & Muggeridge (1988)
		4.4H	Lepparanta and Hakala (1992)
Keel depth	*H*	4Hs - 5Hs	Dolgopolov et al. (1975)
		3.96Hs	Burden and Timco (1995)
		5.8Hs	Kankaanpaa (1989)
		14h - Beaufort, 25h - Bering	Vaudrey (1983)
		7Hs-12Hs	Palosuo (1975)
		3Hs-9Hs, 4.5Hs (av)	Kovaks (1972)
		H distribution is exponential	Weeks and Kovacs (1970)
Keel porosity	*e*	mean 29% and std. dev. 5%	Kankaanpaa (1989)
		29%	Lepparanta and Hakala (1992)
		13% + 0.72x(Sail porosity)	Burden and Timco (1995)
Keel angle	*a*	32 deg	Kankaanpaa (1989)
		32 deg	Cammaert & Muggeridge (1988)
		mean = 27.6 deg, std.dev. = 13.9 deg	Burden and Timco (1995)
		32 deg	Weeks and Kovacs (1970)
		15-60 deg, 39 deg (av)	Palosuo (1975)
Keel Shape		Trapezoidal	Dolgopolov et al. (1975)
		Triangular for large ridges	Lepparanta and Hakala (1992)
		Trapezoidal for small ridges	Lepparanta and Hakala (1992)
Sail width	*Ws*	Ws/h = 17.1/(h^0.5)	Tucker and Govoni (1981)
Sail height	*Hs*	2.2 h^0.5	Kankaanpaa (1989)
		H/3.96	Burden and Timco (1995)
		H/5.8	Kankaanpaa (1989)
		3.69 h^0.5	Tucker and Govoni (1981)
		Spatially highly variable	Tucker and Govoni (1981)
Sail porosity		19%	Lepparanta and Hakala (1992)
		21%	Kankaanpaa (1989)
		25 - 33%	Veitch et al. (1991b)
		30%	Gladwell (1975)
		36 - 43 %	Keinonen (1977)
Sail slope angle		21 deg	Kankaanpaa (1989)
		10-50 deg, 30 deg (av)	Palosuo (1975)
		25 deg	Weeks and Kovacs (1970)
		25 deg	Wright et al. (1978)
		10-55 deg, mean = 24 deg	Kovacs (1972)
		8.8-51.3 deg, mean = 26.1 deg	Tucker and Govoni (1981)
		mean = 20.4, std.dev. = 11.5 deg	Burden and Timco (1995)
Keel brine salinity	*S*	40 - 120 ppt	Weeks and Kovacs (1970)
Keel block Temp.		-0.2 C throughout keel (freezing point)	Lepparanta et al. (1995)
Keel block flex. st.		0.2-0.4 MPa	Weeks and Kovacs (1970)
Ice block length	Li	0.6-0.9 m	Lepparanta and Hakala (1992)
		1.5 x width, 2.8 x thickness	Veitch et al. (1991b)
Ice block thickness	*h*	0.1-0.3 m	Lepparanta and Hakala (1992)
		0.15-0.19 m	Veitch et al. (1991b)
		0.15-0.2 and 0.5-0.6 m	Weeks and Kovacs (1970)
Ice block area		0.67 e^(1.86h) or 4.48 h^2	Tucker and Govoni (1981)
Ice block size distn.		Tight, maximum length < 2 times average	Lepparanta and Hakala (1992)
		Log-normal	Veitch et al. (1991b)
		Bi-modal	Weeks and Kovacs (1970)
		Multi-modal	Tucker and Govoni (1981)
Ice block shape		Platy, rounded and porous	Lepparanta and Hakala (1992)
		Deteriorated, rounded	Weeks and Kovacs (1970)
Ice block placement		Random, large blocks at bottom	Lepparanta and Hakala (1992)
Ridge spacing		Distribution is exponential	Weeks and Kovacs (1970)

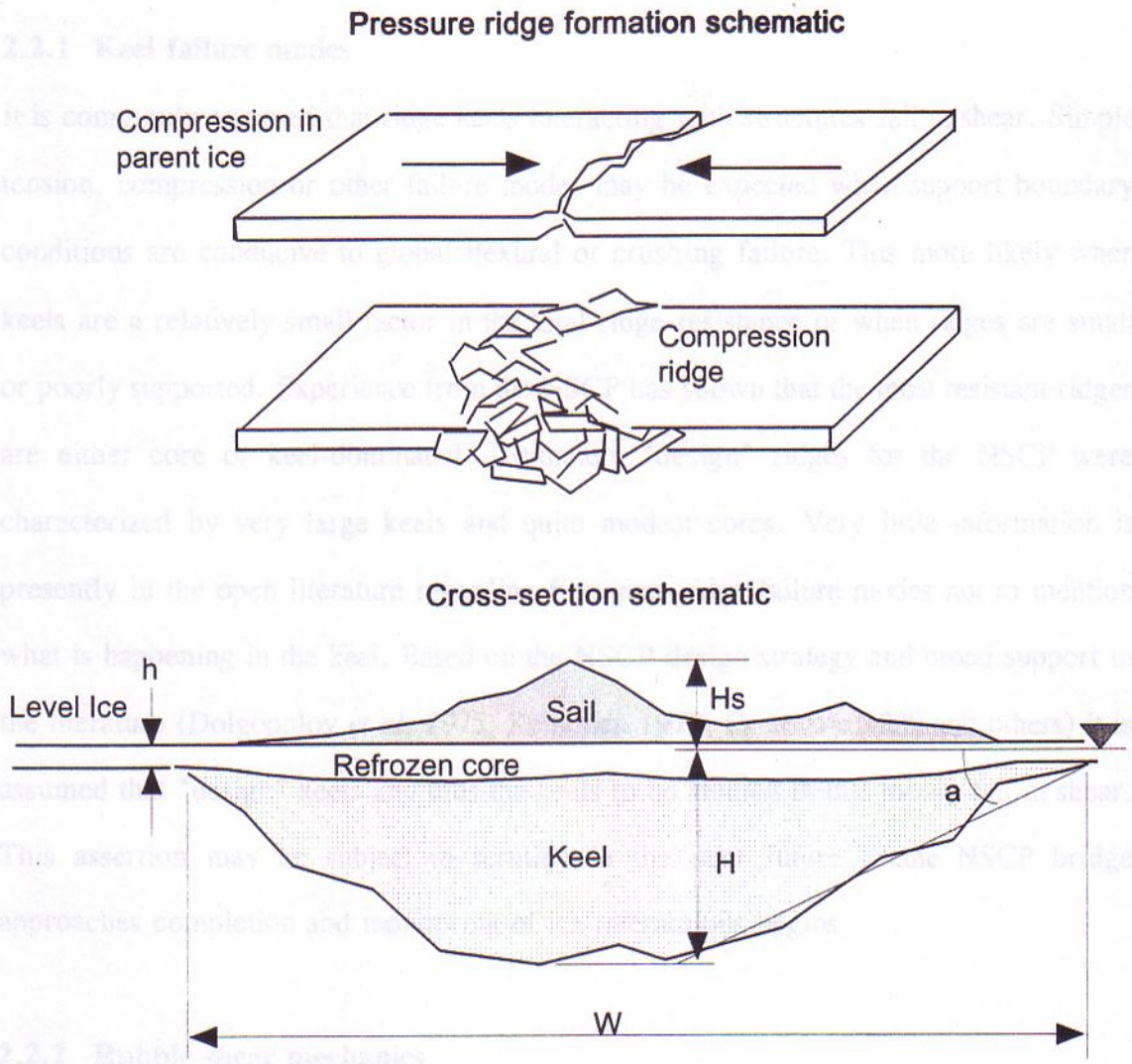

Figure 2.1 Schematic of first-year ridge formation and cross-section.

2.2 Ice rubble strength

2.2.1 Keel failure modes

It is commonly assumed that ridge keels interacting with structures fail in shear. Simple tension, compression or other failure modes may be expected when support boundary conditions are conducive to global flexural or crushing failure. This more likely when keels are a relatively small factor in the total ridge resistance or when ridges are small or poorly supported. Experience from the NSCP has shown that the most resistant ridges are either core or keel-dominated. Ultimately "design" ridges for the NSCP were characterized by very large keels and quite modest cores. Very little information is presently in the open literature regarding first-year ridge failure modes not to mention what is happening in the keel. Based on the NSCP design strategy and broad support in the literature (Dolgopolov *et al.* 1975, Keinonen 1979, Croasdale 1980 and others) it is assumed that "design" keels and thus the keels to be studied in this thesis, fail in shear. This assertion may be subject to scrutiny in the near future as the NSCP bridge approaches completion and monitoring of ice interactions begins.

2.2.2 Rubble shear mechanics

Although ice rubble has been shown to be a multi-phase, highly complex material, it accumulates predictably in specific configurations (keels for instance). Since it is practically incoherent during formation frictional resistance must be active. In time, blocks bond which makes rubble coherent also so that both frictional and cohesive qualities coexist (Prodanovic, 1979).

Friction is the tangential force required to move one surface past another and is defined for static and kinetic conditions. For a granular material *internal* friction results from the slip movement between the surfaces of "blocks" of fixed particles (Bridgwater, 1987). For soils these regions, termed *failure zones*, are typically about ten particle diameters in width and are actually made up of substantial particle rolling, sliding and in some cases attrition (both fragmentation and abrasion). Typically, internal friction is primarily influenced by density and grain packing and to a lesser extent dependent upon a sliding friction component. The reason is that considerable *interlock* occurs between grains so that for sliding and rolling to occur grains must be lifted over one another or else fail in flexure, shearing or crushing. Sliding friction is mostly a material property which varies with surface roughness, pressure, speed and the presence of interstitial water, gases and chemicals, but interlock and thus internal friction, varies with gradation and densification. When sheared, granular materials often undergo volumetric change (dilation) due to the effects of interlock and grain packing (Figure 2.2).

Cohesion is the finite shear strength a granular material possesses when it is not subjected to confining stresses. In ice rubble this property is believed to arise from freeze-bonding between blocks. Freeze-bonding has been shown to be a function of contact pressure, contact period, temperature, salinity, size and shape of the ice blocks, and other factors.

Shear resistance in granular materials is influenced by the presence of fluid in pores. Surface tension acts only when air and water are present together and is not expected to play a role in rubble shear mechanics. On the other hand fluid dynamics may be important. For instance, increased pore pressures have been shown to enhance and reduce shear resistance in soils. At high speeds a submerged dilatant soil may have

appreciably higher shear resistance in accordance with reduced pore pressures (resulting from volume expansion and lower permeability). When bulk compression takes place, pore pressures may be enhanced which causes effective stresses between particles to be relieved, diminishing shear resistance. For ice rubble in keels, open channels between blocks are large so permeability is very high and pore pressure is not expected to vary much. However, with increased particle scale, the drag and inertia of blocks and suction between adjacent ice plates may become significant. A simple calculation reveals that an average sized ice block (0.6 x 0.45 x 0.15 m) ascending perpendicular to its principal axis in water has a terminal velocity of 0.5 m/s (free fall in air would be 45 m/s). Fluid flow around a structure or through a keel during failure can exceed this *critical* velocity causing suspension. The degree of suspension will depend on the state of coherent bonds between blocks. More will be said on this topic later in the thesis.

2.2.3 Yield criteria

At low loads or loading rates and before shear failure, rubble may behave visco-elastically, like a highly porous solid ice. When sheared appreciably, though, unconsolidated ice rubble deforms plastically since the change in shape is irreversible. At failure, behaviour has been shown to be neither *perfectly* plastic (Tresca-Saint Venant condition) nor elastoplastic (as per Prandtl material). The two limiting states or plastic failure theories most relevant to the study of soil mechanics are Von Mises and Mohr-Coulomb. The Mohr-Coulomb model is the most commonly used limit states model in soil and ice rubble mechanics. It was first proposed as a hypothesis of the shear strength for soil by Coulomb (ca 1773) as

$$\tau = c + \sigma_n \tan\phi \qquad (6)$$

where τ is the shear resistance resulting from the slip movement between two "surfaces" within a soil, c is the cohesion of the soil, σ_n is the normal stress on the slip surface and ϕ is the angle of internal friction. Mohr later presented a similar generalized theory and so the limiting state plasticity model became known as Mohr-Coulomb.

The widespread acceptance of the Mohr-Coulomb model has apparently resulted from observations in laboratory tests for ice rubble (Keinonen and Nyman 1978, Prodanovic 1979, Hellmann 1985, and others) that show linearly increasing yield strengths with increased confining pressure (Figure 2.3). Most experiments have also indicated a non-zero cohesive intercept when shear strength data is plotted against a normal stress. Some researchers argue that the Mohr-Coulomb failure criterion may not be appropriate for modelling ice rubble because the internal friction angle and apparent cohesion are a function of normal stress (Ettema and Urroz, 1989). Many researchers would agree that stress history influences the rubble strength and that failure criterion are considerably influenced by many other environmental conditions. Never-the-less the Mohr-Coulomb approximation prevails as it is a simple and effective interpretive tool for laboratory testing and allows the easy adaptation of (Mohr-Coulomb based) soil failure mechanics to keel load models.

In situ materials often have shear stresses on the octahedral plane since all three principal stresses are most often not equal ($\sigma_1 \neq \sigma_2 \neq \sigma_3$). The intermediate stress, σ_2, is commonly ignored, however, or assumed equal to σ_3. The resulting two-dimensional stress state greatly simplifies computation efforts without too much error in most cases (Bowles, 1984).

Considering the two-dimensional case further the equations for normal stress, σ_n, and shear stress, τ, on an arbitrarily inclined plane passing through a rubble body are:

$$\sigma_n = \frac{\sigma_1+\sigma_3}{2} + \frac{\sigma_1-\sigma_3}{2}\cos 2\theta \quad ; \quad \tau = \frac{\sigma_1-\sigma_3}{2}\sin 2\theta \qquad (7)$$

which were first recognised by Mohr (1882) as those representing a circle of radius $(\sigma_1-\sigma_3)/2$ and origin $(\sigma_1+\sigma_3)/2$. The Mohr's circle diagram is a graphic means of identifying the stresses at a point as shown on the right-hand side of Figure 2.4.

Early researchers noted that in a triaxial compression test the axial stress σ_1, at failure depends on cell pressure $\sigma = \sigma_3$. Successive tests at different σ_3 stress levels provide more values for σ_1 and are sufficient to draw a series of Mohr circles. The failure shear strength as a function of normal stress could be reasonably well predicted from the line (or envelope) drawn tangent to the circles as shown in Figure 2.4. The Mohr-Coulomb failure criterion in two dimensions is the equation representing this line. Typically at least three tests are performed for averaging to get a representative value for slope, ϕ, and intercept, c.

A triaxial cell (as per Wong *et al.* 1987) for controlled confinement tests is the most rigorous of all procedures for determining Mohr-Coulomb failure criterion but is also the most complicated and expensive. A biaxial cell (plane stress) has been used by Sayed (1989) whereby controlled ice rubble confinement pressure in one direction, perpendicular to an increasing normal stress, was achieved (Figure 2.4b). Direct and simple shear devices in a variety of shapes, sizes and orientations are most commonly used for testing shear strength (Figure 2.4c and 2.4d). Direct shear involves the

placement of a sample in a box or cylinder which is split so as to allow relative tangential motion of the two parts. A pressure is applied normal to the slip plane of the sample through any number of means - pneumatic bladder, hydraulic pistons, weight placement etc. Direct shear test results are plotted on a graph to yield the best fit failure envelope since the shear stress itself is measured "directly" (Keinonen and Nyman 1978, Prodanovic 1979, Hellmann 1984, and others). Some consider this to be a plane strain test since only lateral and vertical motions can take place. Simple shear tests attempt to produce a state of pure shear for samples undergoing plane strain (Urroz and Ettema, 1987). The problems with the direct shear device (changing sectional area and assumed failure surface orientation) are partially overcome in simple shear devices although stroke length is reduced and equipment is more complicated.

Often the repose angle of an accumulation of a cohesionless granular material is considered a lower-bound estimate of internal friction angle. For instance, when carefully poured into a pile, sand is close to a minimum density state and usually has a repose angle around 30° which is around the low density internal friction angle determined from direct shear tests (Bowles, 1984). For cohesive granular materials this approximation does not apply.

2.2.4 Investigations of ice rubble shear strength

Summaries of laboratory investigations into the shear behaviour of ice rubble are found in Wong *et al.* (1987), Ettema and Urroz (1989), Case (1991), Chao (1993) and others. Few references citing full-scale rubble experiments or strength tests are available. Lepparanta and Hakala (1992) and Coon *et al.* (1995) describe field trials where ridge keel strength was tested and others have estimated strength from observations in the field.

Lavender (1973) for instance describes obtaining estimates of friction angle and cohesion from river ice jams, and Williams *et al.* (1993) describe keel resistance while coring ridges in the Northumberland Strait. Some inferences can be made by observation of rubble repose angle shown earlier to be around 27° on average for keels. Laboratory experiments dominate the literature record of rubble shear strength measurements. A collection of references with reported conditions and results are listed in Table 2.3. Some experiments on solid ice are also listed on the bottom of the table as a reference for extreme upper-bound strengths for highly consolidated rubble (as in multi-year ridge keels).

Few obvious trends emerge as one scans the data columns of Table 2.3. Rubble shear strength shows huge variations from source to source with reported ranges of internal friction angle, ϕ, from 11° (Weiss *et al.* 1981) to 65°+ (Loset and Sayed, 1993) and cohesion, c, anywhere from 0 (Urroz and Ettema, 1987) to as high as 10 or 20 kPa for cold and dry ice (Sayed, 1987). High values for both rarely coincide. Reconciling these results with those for other materials proves to be difficult even for friction angle which is seemingly less dependent upon parent material than cohesion. For example, gravels have internal friction angle varying anywhere from 32° to 36° for loose accumulations and from 35° to 50° for dense packing. These values are comfortably bounded by the extremes reported for ice rubble. Curiously, Urroz and Ettema (1987) found the internal friction angle of polyethylene blocks to be around 35° and that for similarly sized and shaped ice blocks to be 51° when packing densities and testing procedures were identical. Remarkably, Lepparanta and Hakala (1992) report full-scale friction angles to be less than 10° though an adequate explanation is not given.

Clearly, ice rubble shear strength is **state-dependent** and **not unique**. There are many control variables, trends are weak, and multicollinearity is highly probable. Regression analyses on this sort of data are complicated since testing and analysis procedures vary widely. For example, many different shear apparati, rubble types and handling procedures have been used. Compounding the difficulty is an incomplete record of control parameters for each program. In this thesis multiple regression techniques are used to test the relevance of control parameters and to develop best-fit empirical relations to the shear strength data available in the literature.

Table 2.3 Review of ice rubble shear information in the literature.

Author(s)	Ice Properties	Test type	Maximum confine. pressure kPa	Temp	Porosity %	Maximum Layer Depth mm	Speed mm/s	Friction angle deg	Cohesion Pa	Notes
Cheng and Tatinclaux (1977)	Fresh ice: 2 types 38x32x8 mm blocks, and crushed ice.	Direct vert. 2-sided 244-609 x 450 mm Rotary vane shear approx. 250 mm dia.	0.087	Submerged 0 C	-na-	90-275	0.25-6	0-80+ (42-50 from Mellor 1980)	0-3350	Wide range of tests Merino (1974) records similar result with same apparatus (cit. Cheng and Tatinclaux)
Keinonan and Nyman (1978)	Saline parent sheet = 20 mm Flex. strength scaled 1:10 - 1:50 Blocks: h x 2.5h x 3.2h Max block = 8h Many small pieces by test end Model ice elas. higher than natural	Direct horiz. shear 300 mm square box	1.47	Submerged 0 C	32-37	300	"Slow" by hand	47	11.3	
Prodanovic (1979)	Uniaxial freezing saline water Strength scaled 1:50 , thick = 19 mm and 38 mm, max. block size = 8h Flexural str. = 18 kPa, E=5.9 MPa Compressive str. = 25.5 KPa	Direct vert. shear 300x457 mm box	2.7	Submerged 0 C	38	304 304	Rate varied 0.1-8	47 53	250 560	Parent sheet h=19 mm Parent sheet h=38 mm
Weiss et al (1981)	Saline parent sheet = 80 - 200 mm Flexural strength = 30-80 kPa Strength scale approximately 1:10 Max block size: 4h water S = 50-60 ppt, ice S = 10-18 ppt	Direct vert. shear 1 m x1.5 m	31	Submerged -2.5 to -5 C	19-50	1000 1000 1000 1000 1000 1000	4 25 3 24 5 25	13 11 26 25 34 34	1700 1200 2300 1400 4100 3400	Parent sheet h=80 mm Parent sheet h=80 mm Parent sheet h=150 mm Parent sheet h=150 mm Parent sheet h=200 mm Parent sheet h=200 mm
Hellmann (1984)	Three types: Fresh ice chips: 10-20 mm Fresh ice cylinders: 30-50 mm Urea doped columnar: individual grains	Direct vert. shear 'cross-shaped' 2 sides at 0.7x0.7 m 1 m^2 total	4.2	Submerged 0 C	-na-	700 700 700 700	10.9 1.6 10.7 10.7	54 61 44 64	580 420 280 0	Ice chips Ice chips Cylinders Doped
Fransson& Sandkvist (1985)	Three ice types: Fresh: h = 39, Lx = 110, flex. = 1000KPa Fresh: h = 46mm, Lx = 8 mm, flex. = 780 kPa Saline: 6 ppt ,h = 52 mm, Lx = 4 mm flexural strength = 38 kPa	Direct horiz. shear 500 mm square	3	Submerged Ice = 0 C water = 2 C	20	500 500 500	10 10 10	34 14 13	550 450 240	Parent sheet h=39, length=110 mm Parent sheet h=46, length =8 mm Approx results from saline. Parent sheet h=52, length =4 mm
Urroz and Ettema (1987)	Three sizes fresh ice and 1 plastic: small: 18x18x18 mm medium: 38x32x16 mm large: 95x95x38 mm polyethylene: 38x31x9.5 mm	Simple shear Rubble is vertically unconstrained 530x609 mm	0.48	Floating layer, 0 C	36-41	76-229 76-229 133-200 152-229 152-76	2 2 2 2 2	36.6 51.6 30.5 51 35	0 0 0 0 0	small (blocks) med (blocks) large (blocks) large (blocks) plastic (blocks)
Sayed (1987)	Fresh ice: 30 mm cubes Not submerged	Biaxial plane strain Isotherm. cold, dry 500x300x300 mm	Confining press. = 35 max. = 130	-10 C	Initial 40-46 Final 30-40	-na-	0.032-0.85	27-45	10000 - 20000	

Table 2.3 (Continued)

Author(s)	Ice Properties	Test type	Maximum confine. pressure kPa	Temp	Porosity %	Maximum Layer Depth mm	Speed mm/s	Friction angle deg	Cohesion Pa	Notes
Wong et al. (1987)	Crushed fresh ice cubes Max size = 4.75 and 9.5 mm (3 mm av.) Uniformity coefficient 2.8 - 4.0	Direct horiz. shear 300 mm square	(Very high) 140	-2 C Brine & Dry	Initial 41-5	200	Very slow 0.0098-0.046	No peak - monotonic increase		Gale et al. (1986) similar testing arbitrary max selected for phi-c but tests similar to these
Case (1991)	EGADS (doped fresh) ice sheet 30 mm thick, brocken into blocks 3.2h average length, 8h maximum size	Direct vert. shear 600x450 mm box	2.41	Submerged 0 C	34-37	450 450 450 450	1 1 1 1	48.9 37.6 34.8 27.2	523 597 674 824	7.5 hrs warmup 8.5 hrs warmup 10 hrs warmup 11 hrs warm up
Lepparanta and Hakala (1992)	Unknown ice type (scale =1:13) 15 mm thick parent sheet	Direct horiz. shear 800x500 mm box Punch tests 150 mm	1.5	Submerged 0 C	20	400	-na-	8.4	800-2400	Punch and direct shear results Reported results unclear
Erantl et al. (1992)	Fine grained model ice (FG,FGX) Scale 1:40 to 1:50, E = 20-30 MPa	Shear box	-na-	-na-	-na-	-na-	-na-	34 30	350 2000	Average for loading rate Amount of slush and deter-ioration of rubble tested
Sayed et al. (1992)	EGADS (doped fresh) ice sheet 30-40 mm thick, brocken into blocks max. size = 20-25 cm, min. size = 5 cm Submerged tests reported here	Biaxial plain-strain 1 m x 1 m x 0.5 m vert. shear zone	100	Air = -2 C Wat. = -0.3 C	24-34 or wet tests	500	0.27-5	47.7 59.7 48.4 30.6	0 0 400 333	Strain ratio:-.23 first 10 kPa only Strain ratio:-.51 first 10 kPa only Strain ratio:-.23 first 10 kPa only Strain ratio:0.0 first 10 kPa only
Loset and Sayed (1993)	Freshwater ice blocks ranging from 25 mm to 130 mm dry and wet tested	Biaxial plain-strain 1 m x 1 m x 0.5 m vert shear zone	90+	Dry = -2 Wet ice = -2 Water = 0	Initial 36-39	500	3.34-5.3	dry 37-65 wet higher than dry	- na -	Tested different size distributions and varied strain ratios
Lehmus and Kama (1995)	Fresh water ice sheet sawn into parallelepipeds approx. 40x150 mm largest = 300 mm	Direct horiz. shear 800x960 mm square below refrozen layer	1.6	Submerged -10 C for varying durations	28-42	800	20 & 10	- na -	- na -	Consolodation time and temp. varied at constant pressure
Cornett and Timco (1996)	Saline ice parent sheet = 0.5% salt by wt. h = 10 cm, pieces broken by hammer to <10cm in length - varying in size, angular in shape	Biaxial plain-strain 1 m x 1 m x 0.5 m vert. shear zone	60	Dry -na- Ice = -10 C Water = 1 C	- na -	500	4.0-5.3	45-70 Saline higher than fresh	- na -	Friction angle decreases with confining pressure

Table 2.3 (Continued)

Author(s)	Ice Properties	Test type	Maximum confine. pressure kPa	Temp	Porosity %	Maximum Layer Depth mm	Speed mm/s	Friction angle deg	Cohesion Pa	Notes
FULL SCALE										
Lavender (1973)	Apparent cohesion from large-scale river ice jams	Analyzed from data						Not publ.	0-3800	
Lepparanta and Hakala (1992)	Baltic first-year ridge keels	Punch shear through keels	12 kPa (11.7 m keel depth)	Submerged	23-33	3300-1170	Very slow <1 mm/min		1700-4000+ 3400	Total shear strength reported Median for keel depth =3.9 m
SOLID ICE										
Roggensack (1975)	Solid columnar freshwater ice	Large shear box	1.49	-2.5 C	0	-na-	0.06-0.12	22.8 25.2	500000 750000	Peak strength Ultimate strength
Zanegin et al. (1995)	In situ sea ice	Direct shear box	3 MPa	0 to -20 C	0	-na-	10^-3 to 10^-1 /s	up to 56	0.3 - 1.2MPa	Range of results given

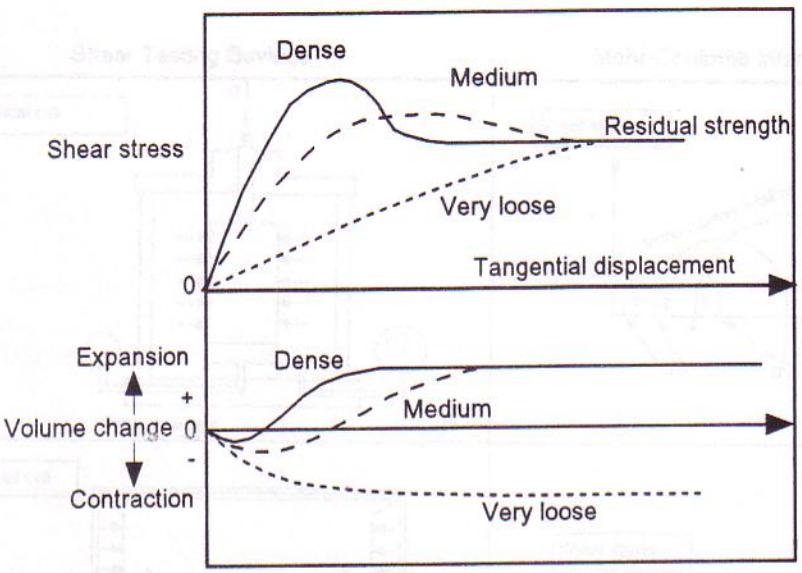

Figure 2.2 Volumetric change of a granular material undergoing shear.

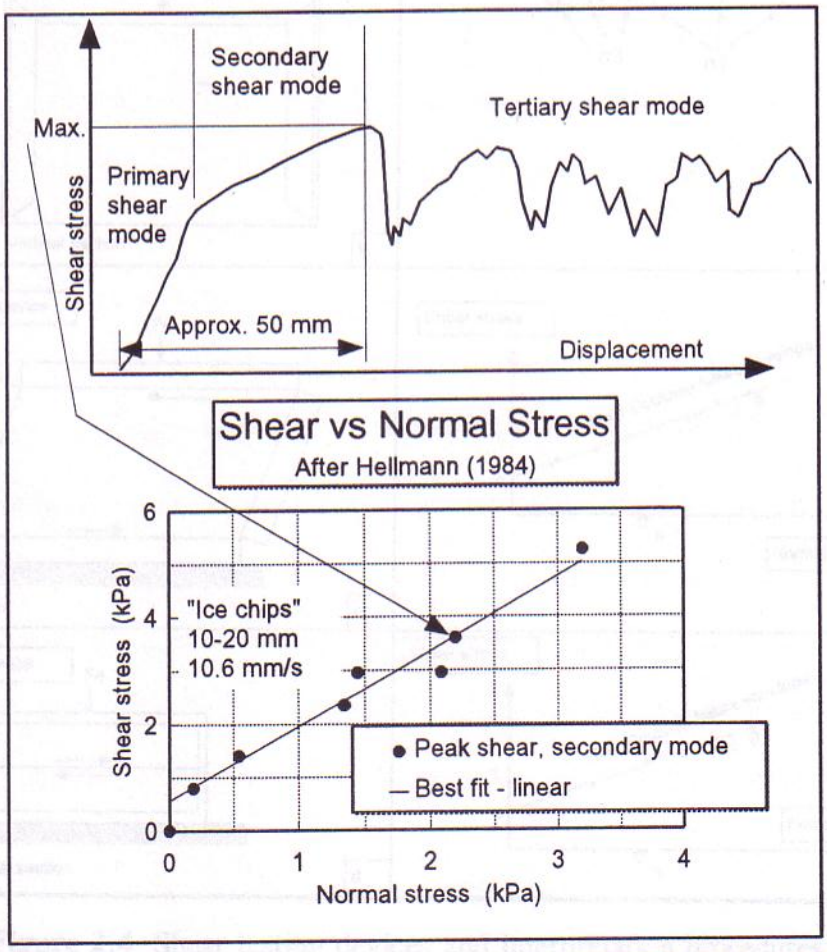

Figure 2.3 Shear behaviour of ice rubble (after Hellmann, 1984).

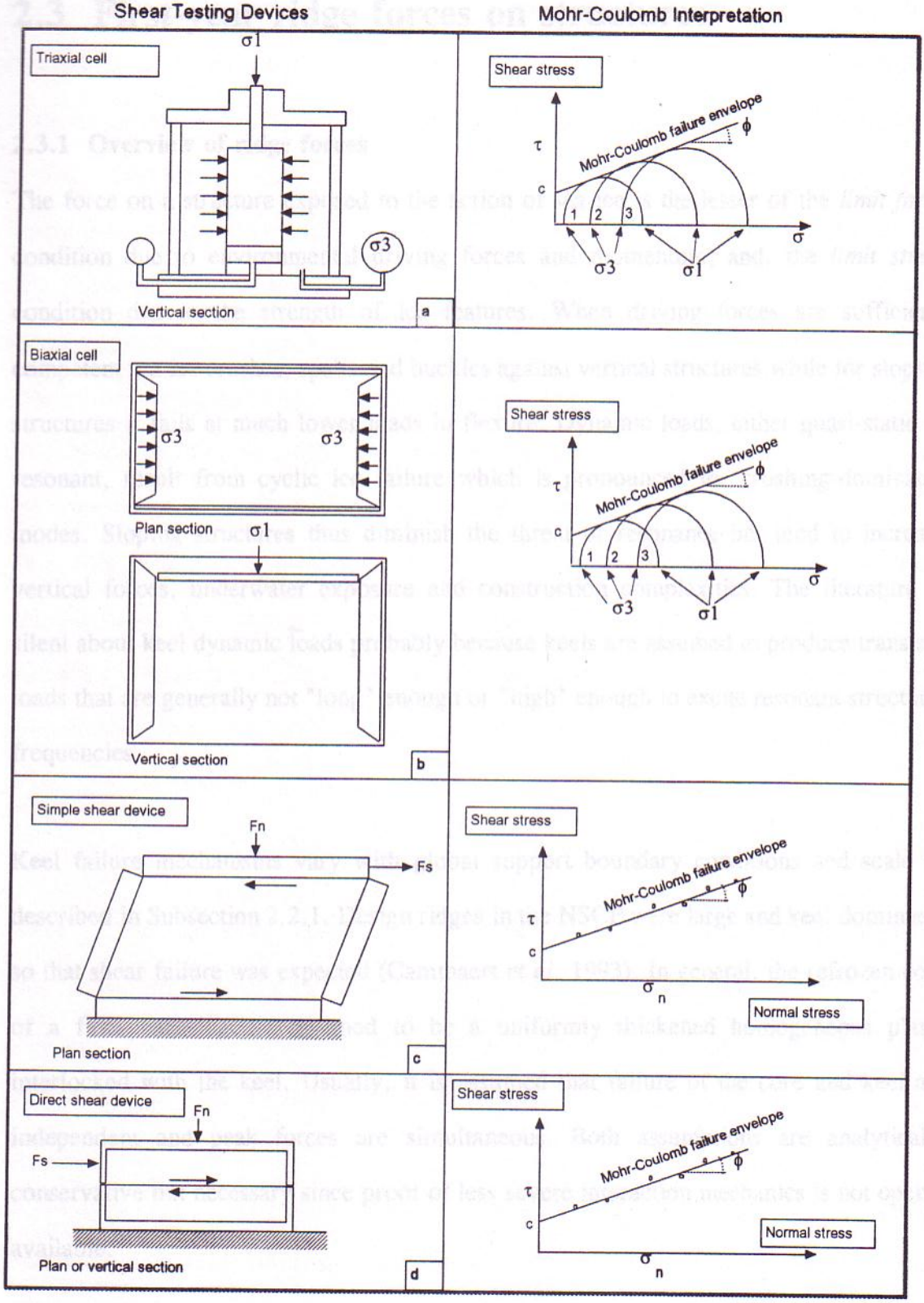

Figure 2.4 Shear testing devices and interpretation procedures.

2.3 First-year ridge forces on structures

2.3.1 Overview of ridge forces

The force on a structure exposed to the action of sea ice is the lesser of the *limit force* condition due to environmental driving forces and momentum, and, the *limit stress* condition due to the strength of ice features. When driving forces are sufficient, competent sea ice crushes, spalls and buckles against vertical structures while for sloping structures it fails at much lower loads in flexure. Dynamic loads, either quasi-static or resonant, result from cyclic ice failure which is pronounced for crushing-dominated modes. Sloping structures thus diminish the threat of resonance but tend to increase vertical forces, underwater exposure and construction complexities. The literature is silent about keel dynamic loads probably because keels are assumed to produce transient loads that are generally not "long" enough or "high" enough to excite resonant structural frequencies.

Keel failure mechanisms vary with global support boundary conditions and scale as described in Subsection 2.2.1. Design ridges in the NSCP were large and keel-dominated so that shear failure was expected (Cammaert *et al.* 1993). In general, the refrozen core of a first-year ridge is assumed to be a uniformly thickened homogeneous plate, interlocked with the keel. Usually, it is assumed that failure of the core and keel are independent and peak forces are simultaneous. Both assumptions are analytically conservative but necessary since proof of less severe interaction mechanics is not openly available.

Interpretation of measured ice forces on structures is complicated work. Often strain measurements are indirect or pressures are measured over representative areas, few cases of direct global measurement of loads where ridges interact have been made (and much of that remains proprietary). In the open literature there are some references to either design loads based on field observations or actual measured data. More often than not *ridge factors* are given which represent the increase in level ice load when ridges are encountered. A significant drawback of this factor is the unknown state of the refrozen core which may, at maturity, be twice the surrounding level ice thickness. None-the-less the keel loads can be bounded somewhat by looking at ridge factors. In the absence of any competent core a ridge factor, R_f, is representative of rubble clearing forces alone (as a ratio of level ice resistance). When a refrozen core is similar in thickness and strength to the surrounding ice then R_f - 1 indicates the rubble clearing force ratio (including confinement effects of the refrozen core). Level ice forces on vertical structures are fairly well understood and are often approximated using the generalized crushing force equation

$$F_c = I f_c m_c \sigma_c D h \qquad (8)$$

where I is indentation coefficient, f_c is the contact factor, m_c is shape factor, σ_c is the strain dependent crushing strength, D is structure width or diameter and h is the ice thickness. Values for coefficients are broadly quoted in a number of publications and texts (Cammaert and Muggeridge 1988, Sanderson 1988).

In the following subsections laboratory investigations and field monitoring programs associated with ridge loading are reviewed. The information from the laboratory programs will be revisited later in Chapters 3, 4 and 6 of this thesis.

2.3.1 Laboratory investigations of rubble indentation

Laboratory investigations which simulate either ridge interactions or generic rubble indentation are reviewed in Table 2.4. Cheng and Tatinclaux (1977) and Keinonan and Nyman (1978) investigated the "two-dimensional compressive resistance" of a floating ice rubble layer. In a tank containing floating ice rubble, a full-width vertical plate was translated horizontally giving rise to bulk compressive resistance forces. Load traces indicated peak and residual strengths, while rubble depth and interaction speed influenced results.

Prodanovic (1979) describes the interaction process for a vertical cylinder translating through a continuous floating rubble field.

> "As the model structures penetrated into the rubble field, the rubble was compressed, the compression zone extending up to 1 m in front of the structure (of diameter 0.304 m, and rubble depth 0.28 m). The ice pieces were mostly moving relative to each other and hence the resistance force was mainly frictional. The ice pieces separated in tangential directions and gradually slid around the structure. The rubble field failure was predominantly planar, with little upward and downward ice activity. Large ice pieces were slightly crushed and occasionally split. Thicker rubble fields created small pile-ups and plugs in front of the structure."

The development of surcharge and other transient load mechanisms appears, from this description, to be down-played.

Hellmann (1984) punched a circular plate horizontally through the centre of a floating rubble mass. Though the interaction process at the structure could not be directly observed it is implied that rubble did flow around all edges of the advancing plate (not just a compression test). A ten-fold increase in resistance resulted from decreasing indentation speed from 250 to 1 mm/s.

Rogachko *et al.* (1994) studied ridges both in the laboratory and in the field. From the paper, reviewed in the next section, it is difficult to determine the exact source of the information given. Timco and Cornett (1995) indented simulated first-year ridges in a study investigating ridge loading on the Northumberland Strait bridge piers. The force contribution of the unconsolidated rubble in the keel portion of the model ridges were roughly estimated from global force measurements.

2.3.2 Full-scale ridge load research

This section describes some field programs in which first-year ridge loading was studied. A review of the programs is provided in Table 2.5. These data and other full-scale load issues will be discussed and analyzed in Chapter 7.

Cook Inlet

In a study lasting several years Blenkarn (1970) investigated ice loading on offshore jacket structures in Cook Inlet, Alaska. Pressure ridges which occur naturally around the periphery of many floes in that region were associated with the peak loading events on the structures. The ratios between peak forces and steady forces for uniform floes were in the range between two and three. Similar values for the "pressure ridge factor" were also determined for a test pile in Cook Inlet. Ridge line loads of 878 to 1042 kN/m were

approximated. Blenkarn was able to discriminate between dynamic and static components of the peak force, concluding that the equivalent static peak force ratio with uniform floe force was less than two.

Gulf of Bothnia

This body of work centres on an instrumented light pier "Kemi-1" in the Northern Gulf of Bothnia near the coast of Finland. There, typical annual ice thicknesses are 0.8 m and ridge keels deeper than 12 m are common. The structure is 10 m wide at average water level and has a slope angle of 55°. Krankkala and Maattanen (1984) report Maattanen's use of a ridge factor of 2.5 based on Baltic experience to that date.

Two principal ice failure mechanisms were observed during ice interaction during the first seasons of Kemi-1 operation (1984/85 and 1985/86); one corresponding to low speeds and the other to high speeds (Maattanen 1986). The former involved the ductile bending of the sheet ice with some single ice layer ride-up, the latter process involved bending, crushing and shearing modes leading to a stationary rubble pile at the leading edge of the pier. Rubble clearing on the cone was "efficient" as pieces climbed and flowed around the cone without the formation of a stationary bow. Maximum ice forces were always associated with pressure ridges, the largest of which resulted from an adfrozen grounded ridge stationary for a week in cold weather and then broken up in a storm. Quantitative force measurements remain proprietary so little data have become available, however, loads were lower than expected at the time of publication (1986) leaving Maattanen to conclude that "... earlier predictions of ice failure models against a conical structure have to be modified".

Hoikkanen (1985) noted the formation of an ice "stack" when pressure ridges rode up on the Kemi-1 cone base. As penetration increased there was a strong flow of ice blocks and brash upwards from the inner parts of the ridge. He noted the presence of large ice blocks longer than 3 m and 1.5 m thick which appeared to be the result of two or three level ice layers frozen together. The level ice following the ridge tended to penetrate the rubble pile or rode up on it. Hoikkanen agreed that the loose parts of a pressure ridge can be treated as a granular material and may be analyzed using the principles of soil mechanics. He further observed that if the structure were narrow and vertical it could further be assumed that the consolidated part fails by crushing, although the Kemi-1 cone showed no clear failure pattern emerging; "... sometimes thick rafted ice was bent but some ridges seemed to be crushed completely". He also noted the inability of model tests to reproduce the crushing failure of the level ice and ridge core observed at Kemi-1.

Recently, Maattanen (1994a) discussed the design of a smaller conical light structure for the Gulf of Bothnia. The structure was 2.6 m at the waterline and had a 60 degree cone angle (from horizontal). The results of the load analysis indicate that a 3.0 MN load can be expected from a design ridge keel, this being greater than the load from a 0.8 m thick level ice interaction but less than the 5.8 MN load predicted for a 1.2 m thick rafted ice layer.

Frederking and Sayed (1994) report that Palosuo (1970) estimated the maximum first-year pressure force on a cylindrical caisson to be in the order of 700 kN/m in the Gulf of Bothnia. The block ice thickness was 0.3 to 0.5 m (personal notes of L.W.Gold) but he did not give a ridge size for this estimate. Palosuo did say that the biggest ridges, comprised of blocks with thickness 0.4 to 0.5 m, were 20 m deep therefore the load

estimate is probably for 15 to 20 m deep keels.

Sea of Okhotsk and other Russian temperate seas

Dolgopolov *et al.* (1975) present methods for calculating ice loads on isolated piers of marine structures which include rafted and ridged ice. Their work is based on field, experimental and analytical data. They state that a uniform solid ice sheet is rarely seen in open seas but that ice fields with ridges of different sizes, shapes and directions are much more common. They refer to the use (prior to 1975) of a ridge factor of 2.2 in Canada and the USA as reported by Dinkla and Sluymer (1970) whereas in the USSR a factor of 1.3 to 1.5 has been taken for temperate seas. In their opinion they felt that data then available permitted the refinement of those numbers. New factors were obtained in an ice basin where vertical and cone shaped piers indented ridge formations. The results obtained were as follows: "the magnification factor for the vertical pier made up 1.54 with loose ice blocks in the underwater part of the ridge whereas it amounted to 2.5-2.7 with the ice blocks frozen together. The magnification factor for a cone-shaped pier was 1.45 if ice blocks in the lower part were not bonded together".

In a paper by Rogachko *et al.* (1994) an "ice-hummock" or pressure ridge coefficient was studied in large scale controlled experiments for a continuous rubble field. They based their experimental parameters on field observations from the Sea of Okhotsk. It is reported that the thickness of the middle consolidated portion of the ridge varies within 1 - 1.5 times the level ice thickness surrounding the ridge and the keel is 4-5 times greater in depth than sail height.

In their experiments an extensive rubble field was built in front of an extensive level ice

sheet and the two were systematically indented with vertical rigid cylinders. Results were obtained for two consolidation levels - the case where the refrozen core thickness in the rubble field was equal to the level ice thickness, and the other when it was 1.5 times the level thickness. The experimental results for the two cases were plotted on a graph of ridge coefficient, R_f versus sail height-level ice ratio (H_s/h) from which the following empirical relations were developed:

$$R_f = \frac{F_R}{F_I} = 1.23+0.65\left[\frac{H_s}{h}\right] -0.054\left[\frac{H_s}{h}\right]^2 \qquad (9)$$

for refrozen core thickness equal to level thickness, and

$$R_f = \frac{F_R}{F_I} = 2.07+0.66\left[\frac{H_s}{h}\right] -0.0455\left[\frac{H_s}{h}\right]^2 \qquad (10)$$

for the thickness ratio of 1.5. For example, a given ridge with a refrozen core 1.5 times the level ice thickness and sail height 4 times level ice thickness, the keel would be statistically 16 to 20 times deeper than the level ice thickness (10.6 to 13.3 times the consolidated layer thickness) and the total ridge force would be four times the level ice force. This value corresponds to the asymptotic limit of the ridge factor for the thickness ratio of 1.5 in Rogachko *et al.* (1994). If a ridge has a consolidated core thickness equal to the level ice, and keeping the same sail height ratio, the ridge factor becomes 3, also the limit for that thickness ratio. A factor of 3 implies that the rubble resistance is twice the level ice resistance if similar core and level ice thicknesses equate to similar resistances (when confinement and failure modes are considered).

Beaufort Sea

Field monitoring of first-year ridge interactions with the Molikpaq caisson have recently been revisited in Croasdale *et al.* (1995). Above-water observations indicated that many modes of failure were common but that larger ridges generally failed in shear. Ridge load factors were found to be in the range of 1 to 3 and line forces of 0.5 MN/m for keels interacting with the 100 m structure were suggested.

Frederking (1994) states that the line load (load per unit meter) of a cold strong multi-year floe 7-10 m thick was around 2.5 to 5 MN/m from experience with the Molikpaq in the Beaufort sea. He believes that even a 20 m deep first-year ridge in the Northumberland Strait would not be capable of generating line loads anything near *half* of that for the multi-year floe.

Grounded rubble

Grounded rubble fields which form around some arctic structures have been studied by researchers typically interested in load transmission to the structure (Sayed *et al.* 1986, Marshall *et al.* 1991, Poplin and Weaver 1992 and others). Croasdale *et al.* (1994) review field measurements, physical model tests, laboratory tests and theoretical models for grounded rubble and point out that there are no known cases where ice rubble has reduced structural stability and created a problem. On the contrary, ice rubble has often significantly reduced the transmission of ice loads to structures and can significantly mitigate the potential for dynamic excitation of the structure. A study of the sliding resistance of grounded rubble may provide some upper bound limits on unconsolidated rubble shear strength for ridges though this line of work has not been pursued in this thesis.

Table 2.4 Laboratory rubble indentation tests.

Reference	Range of Structural Width m	Range of Rubble Width m	Range of Rubble Depth m	Range of Rubble Area m^2	Range of Speed m/s	Range of Peak Load N	Range of Fric Angle Phi deg	Range of Cohesion c Pa
Cheng and Tatinclaux (1977)	0.91	Contin*	0.076 -0.22	- na -	0.00015 - 0.0028	19 - 386	46	1
Keinonen & Nyman (1978)	0.3	Contin	0.174	- na -	0.025	24	47	10
Prodanovic (1979)	0.152 - 0.304	Contin	0.09 - 0.28	- na -	0.001 - 0.009	8 - 285	50	500
Hellmann (1984)	0.1	Contin	0.2 - 0.8	- na -	0.001 - 0.25	60 - 600	54 - 61	580 - 420
Rogachko et al. (1994)		Contin						
Timco and Cornett (1995)	0.333	0.8 - 1	0.003 - 0.45	0.002-0.45	0.09 - 0.27	70 - 1900	45	1000

* Contin. means that rubble was continuous in the direction of structure displacement.

Table 2.5 Estimations of full-scale loads based on field observations.

Reference	Location	Structure	Ridge factor	Maximum load	Notes
Blenkarn (1970)	Cook Inlet, Alaska	Vertical cylinders Jacket rig	2-3	878-1024 kN/m	Test pile and full structures tested Dynamics analysed
Dinkla and Sluymer (1970)	Canada	Vertical structure	2.2		Reference from Dolgopolov et al (1975)
Paluoso (1970)	Gulf of Bothnia, Fin.	Vertical, cylinder caisson type		700 kN/m	Includes keel and consol. layer Ridge depth approx. 15- 20 m
Dolgopolov et al (1975)	Sea of Okhotsk	Vertical structure	1.3-1.5		Old ridge factor in USSR
Maattanen (1983)	Baltic, Finland	Vertical structure	2.5		Design recommendation for lighthouses
Maattanen (1994)	Baltic, Finland	Conical ice shield small light structure	2-3	Approx 1 MN/m	Keel, c = 5.0 kPa, phi = 45 deg keel, level and rafted ice models are compared for design
Frederking & Sayed (1994)	Beaufort Sea	Vertical structure		500 kN/m	For first year ice up to 2 m thick
Rogachko et al. (1994)	Sea of Okhotsk	Vertical cylinder	2-4		From lab and field observations Formulas for ridge factor in thesis text
Croasdale et al. (1995)	Beaufort	Molikpaq caisson	1-3		Many modes observed
		Ranges:	1-4	500-1024 kN/m	
		Averages:	2.3	800 kN/m	

2.4 First-year ridge keel load models

2.4.1 First-year ridge modelling

When a ridge interacts with an offshore structure loads are created by the breaking of the core and the clearing of the keel and sail when sufficient driving forces prevail. Engineering analyses of loads often include the sail with either keel or core load models and treat the remaining component processes separately (Prodanovic 1981, Eranti *et al.* 1992, Cammaert *et al.* 1993, Croasdale *et al.* 1995). Though it is understood that the core provides an important boundary condition which influences keel failure, the simultaneity of failure and the interaction dynamics are not well understood. Thus the peak loads resulting from both keel and core models are typically added to obtain a resultant peak.

Croasdale *et al.* (1995) assert that design ridges are keel-dominated in size and strength. The failure of the core is said to change keel boundary conditions reducing confining stresses near the structure and slightly increasing them further away. The change is small however, and the error introduced to the keel model over the entire ridge is negligible. Since the discussion in Croasdale *et al.* (1995) appears limited to a class of structures with upward breaking cones at the waterline these statements must be interpreted cautiously. Nevertheless, if one assumes that the keel is plastic behaving as a frictional granular material and that the core is a rigid plastic brittle solid then the former may retain most of its strength after yielding whereas the latter may not. Thus it is assumed in this study that the influence of core failure on keel processes is not significant enough for most structural configurations to alter the independent approach to keel modelling.

Several modelling practices for first-year ridge keels are investigated in Krankkala and Maattanen (1984), Kitazawa and Ettema (1985), Bruneau (1994) and Croasdale *et al.* (1995). The following section reviews the historical development and demonstrates the variety of approaches to keel modelling.

Dolgopolov et al. (1975)

One of the earliest and most influential modelling approaches proposed for ridge keels is provided by Dolgopolov *et al.* (1975). The authors describe that the model was developed from experimental studies in which the physical patterns of interactions were observed. There is little novelty to the approach, however, as it is, in form, the passive earth pressure equation for retaining structures, written as:

$$F = qDH_{eff}\left(H_{eff}/2\gamma K_p + 2c\sqrt{K_p}\right) \qquad (11)$$

where

$$K_p = \tan^2\left(45+\frac{\phi}{2}\right) \quad , \quad H \le H_{eff} \le H+\frac{D}{2} \quad , \quad q = \left(1+\frac{2H}{3D}\right) \qquad (12)$$

and where F in this and other equations presented here is the maximum longitudinal horizontal force on the structure of width D, H is keel depth, γ is the ice rubble weight, c is rubble cohesion and ϕ is rubble internal friction angle (Figure 2.5a). The suggested adjustments to keel depth for surcharge and to structural width for the spatial behaviour of the ice medium appear reasonable, though little guidance is given in assigning a value to H_{eff}. This is a significant stumbling block for the application of the model since, by example, if the structure is twice as wide as the keel depth then loads may vary by 100% for arbitrary assignments of surcharge. The shape factor, q, in Dolgopolov's approach

is explained by Maattanen (1994) as originating from the contribution of *side wedges*, "a common assumption for the shape of a failure surface in soil mechanics" (Figure 2.5b). The ice rubble buoyancy applicable in this formula is usually assumed to be

$$\gamma = (\rho_w - \rho_i)(1-e)g \tag{13}$$

where ρ_w and ρ_i are the water and ice densities, e is the bulk porosity of the ice rubble and g is the gravitational acceleration 9.81 m/s^2.

Keinonen (1979)

Keinonen (1979) developed a model for ship resistance in first-year ice rubble and brash. Since this situation is analogous in some ways to ridge interactions with stationary structures it is considered here. The assumption of linear Mohr-Coulomb ice rubble behaviour allowed the formulation of a passive pressure model similar to that of Dolgopolov *et al.* (1975) but with attention to a variety of structural geometries. Through equilibrium of forces it was shown that:

$$\frac{F}{D} = 1/2H^2(1-e)(\rho_w - \rho_i)gK_{kf} + HcK_{kc} \tag{14}$$

where

$$K_{kf} = \frac{(\sin\psi + \tan\phi_1\cos\psi)(\sin\theta + \tan\phi\cos\theta)\sin(\psi+\theta)}{[(1-\tan\phi_1\tan\phi)\sin(\psi+\theta) + (\tan\phi_1 + \tan\phi)\cos(\psi+\theta)]\sin\psi\sin\theta} \tag{15}$$

$$K_{kc} = \frac{\sin\psi + \tan\phi_1\cos\psi}{[(1-\tan\phi_1\tan\phi)\sin(\psi+\theta) + (\tan\phi_1 + \tan\phi)\cos(\psi+\theta)]\sin\theta} \tag{16}$$

in which ψ is bow flare angle, θ is the slip plane angle, ϕ_1 is the ice-structure friction angle and ϕ is the internal angle of friction of the ice rubble (Figure 2.6). The value of the slip plane angle, θ, was determined using differentiation to minimize the resistance formula above. While dealing with the complications of bow entrance, stem and flare angles it is not clear how Keinonen deals with the slope of the surcharge or the effective depth over which the bow is said to act. The resistance formula was shown (in Kitazawa and Ettema, 1985) to be altered to account for the slippage of ice rubble under a vessel in the "developed condition" so that the $1/2H^2$ term became Hd where d is the depth of the vessel. However, this adjustment does not conform to the passive pressure state as sketched in Figure 2.6 (where the rubble depth is $H+d$ at the point of failure). Keinonen maintained that in the "developed condition" the total force on a ship was actually the summation of five components:

$$F = F_{su} + F_{sl} + F_{se} + F_{PB} + F_{PS} \tag{17}$$

where the first three represent resistance from upper, lower and end bow slip-planes and the last two are for middle body ship resistance on the bottom and side. It was also suggested that the confining pressure along the vertical end slip planes at the bow was in the neutral state so that

$$\frac{\sigma_h}{(1-e)(\rho_w-\rho_i)gz} = \frac{\nu_p}{1-\nu_p} \tag{18}$$

where σ_h is the horizontal pressure at depth z, and, ν_p is Poisson's ratio. Since adjustments for depth and surcharge are in accordance with ship-like clearing processes, and may be *rule of thumb*, the applicability of Keinonen's formulation to first-year ridge interactions with offshore structures may be limited.

Mellor (1980)

Mellor (1980) developed a passive shear failure model for ship resistance in unconsolidated level brash ice. The form of the model was similar to Keinonen's above when a vertical frictionless plate is considered. The differences are Mellor's treatment of rubble depth, buoyancy and effective bow form. The formulation is given by,

$$\frac{F}{D} = (1+\tan\phi\cot\beta'')\left[\frac{1}{2}H_{ks}^2K_p\left[(1-e)\rho_i g\left[1-\frac{\rho_i}{\rho_w}\right]\right]+2cH_{ks}\sqrt{K_p}\right] \qquad (19)$$

where H_{ks} the full brash depth (keel plus sail), and the value in square brackets is the assumed rubble buoyancy (Figure 2.7). The friction angle and cohesion of submerged brash in water is assumed to be the same as that in air. The factor $(1+\tan\phi\cot\beta")$ represents the effective width of the ship bow in accordance with the formation of a false bow with half apex angle of $\beta"$ (Figure 2.7). The angle $\beta"$ appears to be a function of bow form, bow roughness and assumed failure criteria for the brash. For plain strain indentation in a Von Mises material a flat faced rough indentor produces a false bow with $\beta"=45°$. For Mohr-Coulomb $\beta"=(45-\phi/2)$. For an arbitrary friction angle of 35° the bow factor $(1+\tan\phi\cot\beta")$ becomes 2.34. By comparison the shape factor in the formula by Dolgopolov *et al.* (1975) is 2.34 when $H = 2D$. The similarity suggests the Dolgopolov formulation may be based on a similar approximation.

Croasdale (1980 - 1994)

Croasdale (1980) modelled first-year ridge loads assuming that the ridge keel is comprised of ice blocks held together by buoyancy, gravity and frictional forces alone. Thus the ice keel was said to act as a granular material with an assumed friction angle and no cohesion. A plug-type failure was suggested whereby two parallel shear planes

form at either side of a structure during the initial stages of an interaction (Figure 2.8a). The force required to shear through the rubble keel was determined by vertically integrating shear stress and area through an assumed triangular keel cross-section. Since it was also assumed that no consolidation had taken place a horizontal shear plane was not considered. The formula reduced to

$$F = \frac{2WH^2}{3}\rho g \tan\phi \qquad (20)$$

where F is the peak horizontal force on the structure, W is the keel width, H is keel depth, ρ is the buoyant density of the ice, g is gravitational acceleration and ϕ is the internal friction angle of the keel rubble. Horizontal confining stresses were assumed to be equivalent to vertical hydrostatic pressure, an assumption which suggests a stress state slightly higher than the neutral but short of passive conditions.

If cohesive bonds are sufficient to disable frictional sliding, Croasdale suggested that the force required to shear completely through a triangular ridge keel (as described above) would be

$$F = cWH \qquad (21)$$

Based on a downwards breaking wedge of width D with failure plane pitch angle of 45°, an approach for wider keels or rubble fields for purely cohesive rubble was proposed by Croasdale (1993) as shown in Figure 2.8b and written as:

$$F = c(2HD + H^2) \qquad (22)$$

The force to clear rubble from the path of the structure was also determined as

$$F = \gamma \frac{H^2}{2} W \left(\frac{1+\nu_p}{1-2\nu_p} \right)$$

where ν_p is poisson's ratio, γ is the buoyant weight of the submerged rubble and W and H are the ridge width and depth. However, this was not to be added to the cohesive rupture failure as the two were not assumed to act together. Croasdale (1993) also considered a footing failure for rubble fields (Figure 2.8c). Formulated in accordance with Figure 2.8c it was shown that

$$F = c(\pi DH + \frac{\pi D^2}{2}) \qquad (24)$$

where D is the structure width and also the radius of the failure slip surface. The first term reflects shear along the vertical circumferential slip surface, the second is for shearing on the interface between the ridge consolidated core and the rubble.

Croasdale (1994) updated the friction plug model (from 1980) to include the effects of friction on the underside of a refrozen core. If a horizontal shear plane, of width D, fails simultaneously with the two sides of the plug, the friction plug model becomes

$$F = [WDH/2 + WH^2/3](\rho_w - \rho_i) g (1-e) \tan(\phi) \qquad (25)$$

Prodanovic (1981)

Prodanovic (1981) developed a plasticity upper bound model for ridge forces on vertical (cylindrical and flat-sided) structures. The model, which accommodates both crushing

and shearing, assumes the ice rubble behaves as an elastic-perfectly plastic material, described by the corresponding yield functions, and that the associated flow rule relates current plastic strain rates to current stresses. The model conservatively estimates maximum loads by constructing admissible velocity fields and applying the upper bound theorem of plasticity theory (note that Prodanovic assumes the simultaneous failure of the consolidated level ice zone and the keel rubble in the determination of the maximum ice loads).

Two failure mechanisms commonly observed in first-year ridge model tests are described by Prodanovic as "plug-type" shearing and "gate-type" crushing modes (Figure 2.9). Shearing is the more common failure mode in model tests when the structure diameter is large in comparison to the ridge thickness (ie $D/H > 0.5$). The crushing failure mode follows a classical Prandtl velocity field with ice blocks flowing and clearing on both sides of the indentor in a log-spiral fashion. This mechanism is postulated to occur more often when the structure diameter is small and plain strain conditions are approached.

Prodanovic (1981) assumed that rubble behaves as a Mohr-Coulomb material (homogeneous and isotropic - strength increasing linearly with confinement). A three-dimensional extrapolation of the yield function was applied to construct a rubble force upper bound solution. The formulas reduced to

$$F = 2Ac \qquad (26)$$

for rubble shearing, where A is the keel cross-sectional area and c is the cohesion, and,

$$F = 2cDH\tan(45^o+\phi/2)\left[1+a'\frac{H}{D}\left[1+b'\frac{H}{D}\right]\right] \quad (27)$$

where

$$a' = 0.89[1+1.82(\phi-17^o)] \quad , \quad b' = 0.31[1+2.01(\phi-8^o)] \quad (28)$$

(cit. Croasdale *et al.* 1995) for rubble crushing.

Prodanovic's (1981) work illustrated the dominance of rubble shearing at high aspect ratios (structural diameter to level ice thickness) and the mechanism of crushing providing cut-offs at lower aspect ratios.

Eranti et al. (1992)

In Eranti *et al.* (1992) the authors report that the keel force component of first-year ridge interaction models can be estimated by classic soil mechanics as Prodanovic (1979) did assuming rubble plastic flow shear reaches the Mohr-Coulomb yield criterion. They suggested the use of Dolgopolov's model (attributed to Eranti and Lee in Krankkala and Maattanen, 1984) as a "fair first-estimate" of the ridge keel load if the structure is narrow when compared to the keel. It is pointed out that a more sophisticated analysis taking into account the cohesion profile among other things is required for final design.

When the structural width is large compared to the size of the keel Eranti *et al.* (1992) believe the penetration angle (oblique angle between direction of advance and keel long axis) and keel geometry become important. Eranti *et al.* suggest the use of a *cross-over* load estimating technique in which the maximum keel load is determined as the

intersection of passive and plug failure mode models - computed as a function of penetration into the ridge (Figure 2.10).

According to Allyn (1994), Eranti now uses a Brinch-Hansen "pile" model (Brinch-Hansen, 1961) which represents the ultimate resistance of rigid piles in earth against transverse movement. He has used this model which considers the slope angle of the keel, in the calculation of ice loads for the design of the bridge to span between Denmark and Sweden. Eranti is credited as having calibrated his model based on much Baltic sea ice data. Eranti presently believes, according to Allyn (1994), that there is only one model required which calculates the failure planes as a function of indentation into the ridge, and which he bases on the extensive model testing that he has directed.

Maattanen (1983, 1994b)

Maattanen (1983), as reported in Krankkala and Maattanen (1984), did not use soil mechanics arguments to formulate a ridge load model. He assumed the pressure distribution caused by a first-year ridge against a vertical structure to be comprised of a triangular sail and keel contribution and a uniform sheet ice contribution, apparently all acting simultaneously (Figure 2.11) . The sail height is assumed to be two times level ice thickness, h, and the keel depth is $10h$. The total load due to a ridge (sheet ice and rubble) is obtained by

$$F = F_c + F_{sail} + F_{keel} = F_c + F_c/2 + F_c = 2.5F_c \qquad (29)$$

where F_c is the sheet ice crushing load, F_{sail} is the sail load contribution and F_{keel} is the keel load contribution. Thus the ridge load is dependent only upon the level ice sheet crushing load. This also implied the dependence upon the ice/structure aspect ratio. Maattanen points out that rafted ice (layered ice) contributes only to the level ice portion and that adfreezing (understood here to mean cohesion between blocks) may serve to influence the sail strength independent of the other two factors. Therefore it is concluded in Krankkala and Maattanen (1984) that the above formula may be used but if better estimates of individual components are known then they should be used instead.

Maattanen (1994b) believes that a downward wedge failure model, ie. Dolgopolov *et al.* (1975), is applicable in the case where the ratio of keel depth to structural diameter is small (2 or less). This type of failure model has also been developed by Broms (1964) for the lateral resistance of piles in cohesive soils. Maattanen believes that when the ratio is large one would expect a Prandtl type failure. Actual failure surfaces for first-year ridge keels would have a Prandtl mode at the centre and wedge modes both at the top and bottom (at top if consolidated layer does not restrict it). He goes on to state that the shape factor as used in Dolgopolov's approach will be more complicated in the mixed mode case and it will depend upon H/D. Also a turnover into a shear plug mode is more likely so that ridge ice loads will be lower than the pure Prandtl mode suggests. For the case of a conical structure as in the Kemi-1 lighthouse in the Baltic Sea, Maattanen has concluded that omitting the shape factor from Dolgopolov's model results in more realistic ridge loads but that it is a "good detail" to observe the increased keel depth due to displaced rubble during the initial penetration into the keel.

Maattanen (1994b) reiterates that, in plastic limit analysis, failure surfaces are similar

both in cohesive and frictional materials. He says weaknesses in many keel load strategies include the separation of cohesive effects from frictional effects, the over-simplification of keel and structural geometry (constant depth keel and vertical instead of sloped surface for example) and the use of planar failure surfaces. Maattanen says that one might expect non-parallel failure surfaces and that due to high roughness, the consolidated core bottom will not attract shear plane formation but would cause failure surfaces to curve downwards. This has been independently verified by Allyn (1994) who states that the plug failure plane is not at the underside of the consolidated layer as determined in model tests. According to Allyn, Eranti also believes this to be the case and suggests that it reduces loads by 20% over typical horizontal failure surface calculations.

Hoikkanen

As cited in Krankkala and Maattanen (1984), Hoikkanen (no date given) suggests the formation of a "pseudo bow" in front of the structure which interacts with the oncoming first-year ridge or rubble field (Figure 2.12). He formulates two horizontal load expressions; the first for the sail, and second for the keel, based on soil mechanics. For the sail

$$F_{sail} = \left[1+\frac{\tan\phi}{\tan\beta'}\right]\left[(P_1+P_2)rH_s-(\frac{2}{3}P_1+\frac{1}{3}P_2)H_s^2\cot(90-\alpha)\right] \qquad (30)$$

and for the keel

$$F_{keel} = \left[1+\frac{\tan\phi}{\tan\beta'}\right]\left[(P_3+P_4)rH_k+(\frac{1}{3}P_3+\frac{2}{3}P_4)H_k^2\cot(\alpha-90)\right] \qquad (31)$$

where ϕ is the angle of internal friction, β' is half the leading angle of the pseudo bow (though β' is shown in the paper as the full apex angle, it is likely meant to be half of this), and,

$$P_1 = 2c_s(K_{ps})^{1/2}$$

$$P_2 = 2c_s(K_{ps})^{1/2} + K_{ps}\,\gamma_i\,H_s\,n$$

$$P_3 = 2c_k(K_{pk})^{1/2} + K_{pk}\,\gamma_i\,H_s\,n$$

$$P_4 = 2c_k(K_{pk})^{1/2} + K_{ps}\,\gamma_i\,H_s\,n - min\{(\gamma_w-\gamma_i n)H_k\,,\ \gamma_i n H_s\}$$

$r = D/2$ = radius of structure at waterline,

H_s is the sail height,

H_k is the keel depth,

α is the inclination angle of a conical or an inclined structure from vertical,

$K_p = \tan^2(45 + \phi/2)$ is the passive pressure coefficient for sail (s) and keel (k),

$c_{(\,)}$ is the cohesion of ice mass; subscript s for sail and k for keel,

n is the void ratio of the ridge, and

γ_i and γ_w are the specific weights of ice and water.

There is little reference to the basis of this extensive formulation by Hoikkanen as described in Krankkala and Maattanen (1984). A numerical comparison between different methods done by the latter party suggest that loads computed by Hoikkanen's approach are similar to those of Prodanovic. The study is somewhat confusing, however, with uncertainty about the conditions and parametric values prevailing for each of the models.

Joensuu (1981)

Reference to ice load modelling of first-year ridge interactions with conical structures is made in Krankkala and Maattanen (1984). A formulation attributed to Joensuu (1981) who in turn based the work on ridge piling by Parmerter and Coon (1973) is given as:

$$F \approx 10\rho_w g H_s^2 D + 45\rho g \frac{H_s^3}{\tan(\alpha)} \quad (32)$$

where ρ_w is the density of water, g is gravitational acceleration, H_s is the sail height, D is the structural width and α is the cone angle. The first term calculates the force required to increase the potential energy of the ridge, and the second term calculates the force required to overcome the friction between the blocks in the ridge. The authors avoid explaining what the structure width, D, represents since for a cone this varies with height. Also it is not clear whether or not this model includes level ice failure loads.

Sayed and Frederking (1988)

Sayed and Frederking (1988) propose a calculation model of ice rubble pile-up for three dimensional ridge keel geometries. The formulation can be applied to the case of ridge failure and takes the form of an expression for the wall force in the passive stress state. The only difference is in the (material) constant relating line force to keel depth. The line force model suggested by Sayed and Frederking (1988) is:

$$F = 0.76\gamma H^2 \quad (33)$$

where γ is the buoyancy of the keel H is keel depth and the constant 0.76 replaces $K_p/2$ (a factor decrease of about 4 for ϕ of 35°).

Frederking and Sayed (1994) review the works of Broms (1964) on the lateral resistance of piles in cohesive soils since the formulas Broms developed have been considered for ice rubble/structure interaction. Concern over the use of these formulations arises from the semi-empirical nature of the derivations that assume deflections, pile stiffness, compressibility and interaction geometries that pertain to soils and not ice rubble. The

greatest reservation they have in the use of Broms models is the assumption that piles are imbedded in a semi-infinite "half space" and as a result are highly confined, whereas ridge keels are much less so - leading to different failure modes and lower pressures. They advocate the use of a three dimensional non-linear finite element analysis or a discrete element analysis for a more rigorous solution to the problem.

Cammaert et al. (1993)

The Northumberland Strait Bridge Project provided the research incentive and direction for this thesis. Computing the design loads for the main span piers was a challenge undertaken by C-CORE and then CODA led by A.B. Cammaert. The approach used to model to ridge loads on the piers evolved as the structural design progressed from preliminary to advanced stages. A continuous stream of model updates was produced due to the exceptional scrutiny by a review engineering team, new results from laboratory experiments, new environmental data and ongoing rigorous model analysis. In the end the client was satisfied that the approach and results presented by CODA were sound. The strategy incorporated the Dolgopolov *et al.* (1975) passive failure approach and the updated Croasdale (1994b) frictional plug model in a *cross-over* technique as described in Eranti *et al.* (1992). The algorithm was buried in a lengthy simulation routine which used Monte Carlo sampling and assumed parametric distributions to compute extremal distributions from which return period loads were assessed.

In the *CODA* model both passive and plug models were rewritten as a function of penetration into the keel. Additionally, accommodation was made for the flaring of vertical shear planes across the width of the keel as were observed and reported in Bruneau (1994b) (Figure 2.13). Incorporating these changes into Croasdale's model

resulted in

$$F = [(W-x)D+(W-x)^2\tan(\beta)](\gamma H/2)\tan(\phi) + [W'H-2(x')^2H/W'](\gamma H/3)\left[\frac{1-\sin\phi}{1+\sin\phi}\right]\cos\beta \quad (34)$$

where γ is the bulk weight of the submerged ice rubble, x is the penetration of the structure into the ridge in the approach direction, and primed terms are distances along the flared failure planes at angle β to the direction of travel. The pressure on the divergent side failure planes was assumed to be in the active state.

The passive failure model (from Dolgopolov *et al.* 1975) was rearranged to represent the load as a function of penetration into a symmetrical triangular keel of depth H as follows:

$$F = qD(2xH/W)[K_p\gamma xH/W + 2\sqrt{K_p}\,c] \quad (35)$$

Peak load was said to occur at the point where passive loads exceeded plug resistance whereupon it was assumed a plug failure would occur and stresses would be relieved. This peak was said to act simultaneously and independently of core failure since it could not be proven that they did not. Thus the total ridge resistance was said to be the sum of the instantaneous maximum failure loads of both the core and keel.

Through algebraic manipulation it was shown that a quadratic equation, for which there is a closed-form solution, could be used to solve for the point of intersection between the two models. This adaptation was attempted since it simplified and shortened the probabilistic simulation routine. Complications arose, however, when considerations of alternate keel geometries were necessary so the original iterative technique prevailed.

The assumption of a triangular and or trapezoidal keel form while simplifying many aspects of the model, complicated matters when penetration occasionally went beyond the slope discontinuity before plug failure was attained. Special consideration was required in such cases.

Brown and Bruce (1995)

Brown and Bruce (1995) attempted continuum finite element modelling of first-year ridge keel interactions with vertical structures (both wide, two-dimensional and cylindrical types). They found that loads and failure modes resulting from keel interactions were less dependent on the ice rubble cohesion than the friction angle. The model indicated the dominance of rubble clearing mechanisms, including surcharge accumulations, during interactions and the tendency for shear failure in the keel to stay below the core-keel interface. Results also indicated that the loads were proportional to the square of the keel depth. Unfortunately model uncertainty was estimated to range as high as 40% and profound numerical difficulties were encountered at high strains. Non-linear material models additionally complicated the iteration process for solution equilibrium and as a result the use of continuum finite element procedures was discouraged.

Sayed (1995)

In Sayed (1995) a discrete element model is introduced which simulates ridge keel interactions with cylindrical structures. The principal advantages of the discrete or particle element model over continuum finite element methods are the ability to deal with large deformations and discontinuities which usually arise during failure and the realistic simulation of the interaction conditions between ice blocks. Sayed deals heavily with existing techniques for ridge keel load modelling suggesting that failure mechanisms have

so far been chosen completely arbitrarily and that they involve gross inaccuracies. His preference is for "a more accurate approach" which involves solving a set of governing momentum balance and constitutive equations.

Numerical results indicated a linear force dependency on keel depth and an increase in load as one exchanged a triangular keel with a larger trapezoidal one. "Plug formation" was questioned as a distinct failure mechanism since a continuum of velocities without distinct boundaries was observed in the simulations. It was reported, however, that plugs formed perpendicular to the length of a ridge regardless of the direction of ridge motion. Loads were shown to decrease by a factor of two when keel depth was halved, unlike the result from Brown and Bruce (1995).

The developments in particle element modelling reported in Sayed (1995) hold some promise. As described in Croasdale *et al.* (1995) however, the approach may best be used at this early stage of development as a calibration tool. Some issues which must be addressed include the unverified yet significant velocity dependency reported, inertia effects which do not consider the fluid in which the particles are suspended, and failure modes which do not agree with the model calibration test (in which Sayed compared results with a sand experiment by Bruneau, 1994b). The discrete element model would be improved if simulated interactions which began with the model stationed half way through the keel were to start at the leading edge of the keel. Almost all peak simulation loads are reported by Sayed to have occurred within one meter advance from the ridge centerline which may be a sign that this position is past the point of peak load for some interactions with the full keel cross-section (as demonstrated by most *cross-over* simulations).

Weaver (1995)

Croasdale *et al.* (1995) describe the development of a general passive failure model for ridge keels which incorporates structure slope angle, structure rubble friction angle and keel inertia. Dr. J. Weaver was the principal researcher behind the formulation. From first principles, a force equilibrium was established between adjacent rubble zones which comprise the mobilized rubble leading the penetrating structure. The complex formulation involves the pre-selection of rubble zone shape, flare, pitch and confining pressure, as well as the extent of rubble accumulation and the added mass factor of the bulk ice rubble mass. Ice rubble failure criteria were selected on a friction only or cohesion only basis. The model is written as

$$F = \frac{w+2C_a\left[\frac{Z_h}{2\sin\theta}+F_2\left[\frac{\tan\phi}{C_b}-\frac{\sin\omega\tan(\theta-\phi)}{C_a}\right]+F_1\tan\phi+\frac{c_2}{C_b}+c_1+\frac{c_{12}}{2}\right]}{\tan(\theta-\phi)-\tan(\phi_1+\alpha)} \qquad (36)$$

where

$$C_a=\cos\theta[1+\tan\theta\tan(\theta-\phi)]; \qquad C_b=\sqrt{1+\tan^2\alpha\sin^2\theta} \qquad (37)$$

and Z_h is the horizontal inertia force associated with decelerating the failed rubble mass from the initial ridge speed to zero, written as

$$Z_h = \lambda\Delta M\frac{V^2}{2\Delta x} \qquad (38)$$

where λ is a factor that accounts for hydrodynamic added mass and ΔM is the additional mass of rubble and pore water incorporated into the failure wedge due to incremental penetration, Δx. It is not clear if this factor discounts the fluid dynamic inertia affects (drag) already present when currents free of ice flow past the structure. In the

formulation above, V is the velocity of the ridge and is assumed constant for the entire interaction, F_1 and F_2 are the horizontal forces acting normal to mobilized rubble adjacent to (region 1), and distant from (region 2), the structure, and c_1, c_2 and c_{12} are the cohesive shear strengths of the vertical shear planes for regions 1 and 2 and inclined at angle θ respectively. The weight of the multi-faceted failure wedge, w, is computed separately for each step of the advancing structure.

In Croasdale *et al.* (1995) the model is shown to compare favourably with laboratory results by Bruneau (1994b) and its ability to deal with progressive changes in the failure wedge form, structure slope, wall friction and keel inertia are emphasized. The model possesses a high degree of flexibility and it is not clear how sensitive the model is to some of the input assumptions about which little is known. Though this is presently a stumbling block the model does provide a promising framework for enhanced modelling in the future.

2.4.2 Comparison of models

Several of the models described above have been programmed into a spreadsheet as shown in Figure 2.15. The intention is to investigate the relative performance of various models and to demonstrate the variability between approaches and sensitivity to keel input parameters. Reference to other model comparisons can be found in Krankkala and Maattanen (1984), Croasdale *et al.* (1995) and others. Some models reviewed in the previous section were not suitable for spreadsheet application and as a result were either not included in the study or pre-computed results of specific case scenarios were quoted directly.

There are five scenarios considered in the upper table in Figure 2.15. The first corresponds to an arbitrary default case which is somewhat based on design conditions for ridges in the Northumberland Strait. The shaded blocks in the table indicate the parameters varied for each test while all other terms remain constant. Scenarios 2 to 5 consider a shallower ridge keel, greater cohesion, greater friction angle and broader structure respectively. In the lower table computed force values for each model and scenario are listed. The computed forces are also plotted. The results shows that, for predicted loads, the coefficient of variation across the board for the models shown was in excess of 50% on average. The range of results was greater than twice the average for some scenarios. Constant values for different scenarios (within a row in the lower table) attest to the insensitivity of some models to parametric change.

Despite the significant model uncertainty underscored by the jagged appearance of the horizontal chart, some interesting trends emerge. The average force for all models increases 43% over the default value when structure diameter is doubled. A decrease of 78% occurs when keel depth is decreased by a factor of two. Only an 11% increase is experienced when cohesion is doubled. The sensitivity to friction angle appears to be higher than cohesion though a linear comparison cannot be made.

The apparent lack of consensus amongst models comes as little surprise when one considers the data with which they have been calibrated. Laboratory experiments offer little guidance with hugely varying approximations of rubble shear strength. Field force measurements are scarce and, subject to interpretation, may have a higher degree of variability than the models. Even the simple parametric inputs such as ridge geometry show significant degrees of natural variability; for instance, the standard deviation of the

ridge keel slopes measured in the field was one-half the mean.

Improvement on the state of the art in ridge keel modelling will require an approach that deals with parametric and model uncertainty simultaneously. The combined approach will enable the optimization of a force model, sensitive to parameters proven significant and adapted to a relevant range of ridge boundary conditions.

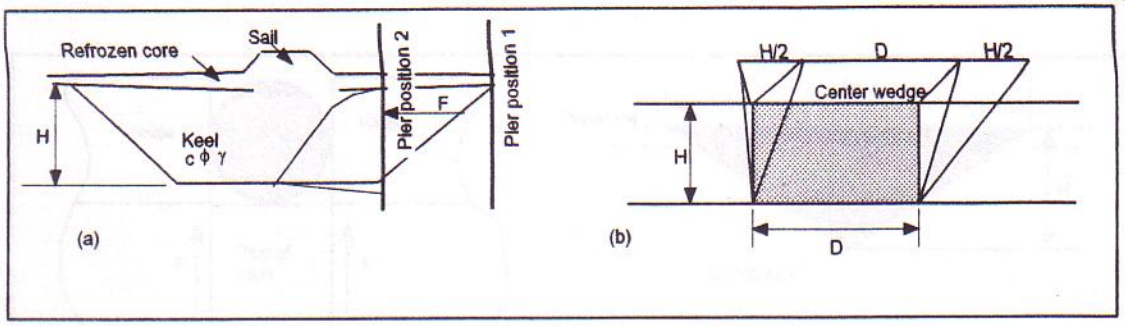

Figure 2.5 Passive failure model after Dolgopolov *et al.* (1975). (a) Interaction sketch (b) effective width model.

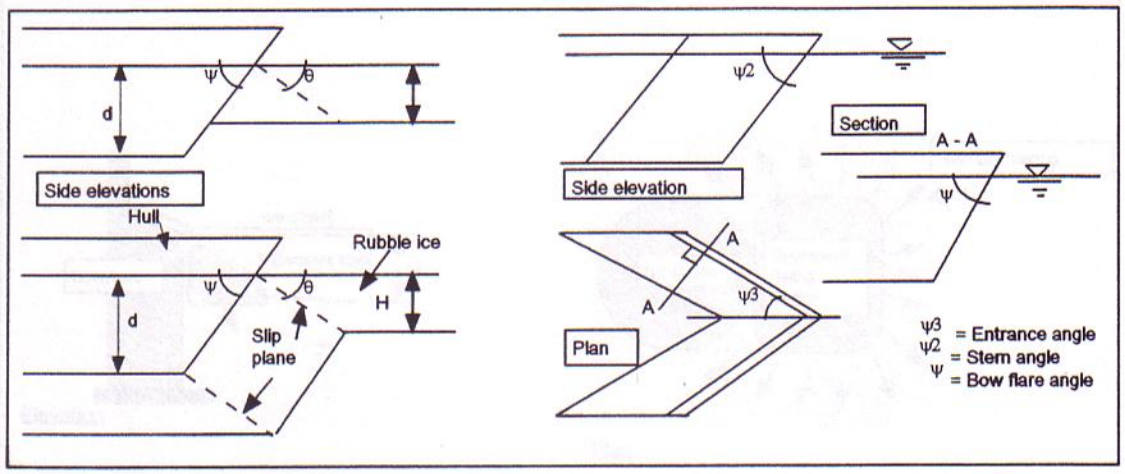

Figure 2.6 Ship resistance in first-year ice rubble after Keinonen (1979).

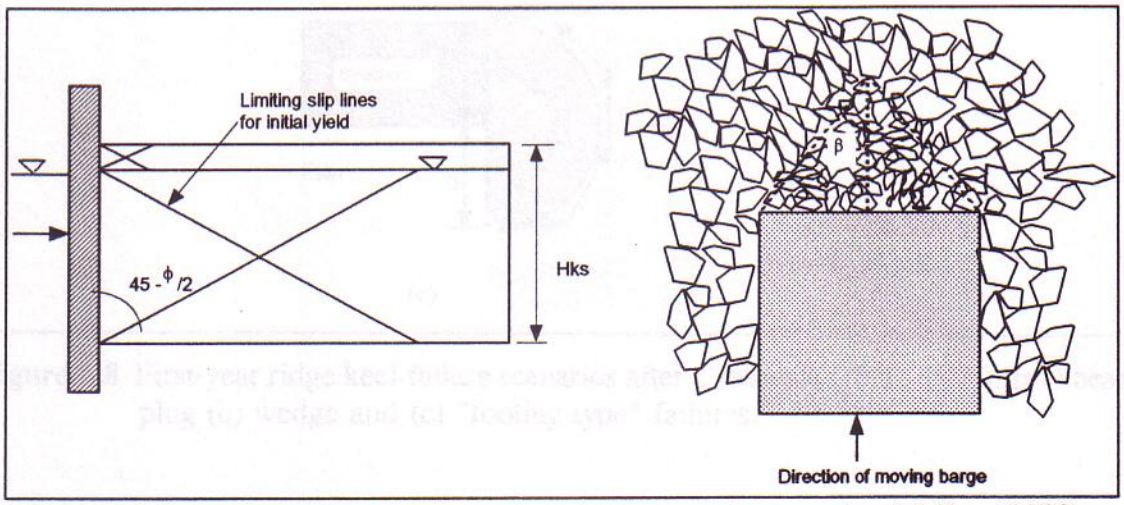

Figure 2.7 Passive shear failure model for ship resistance after Mellor (1980).

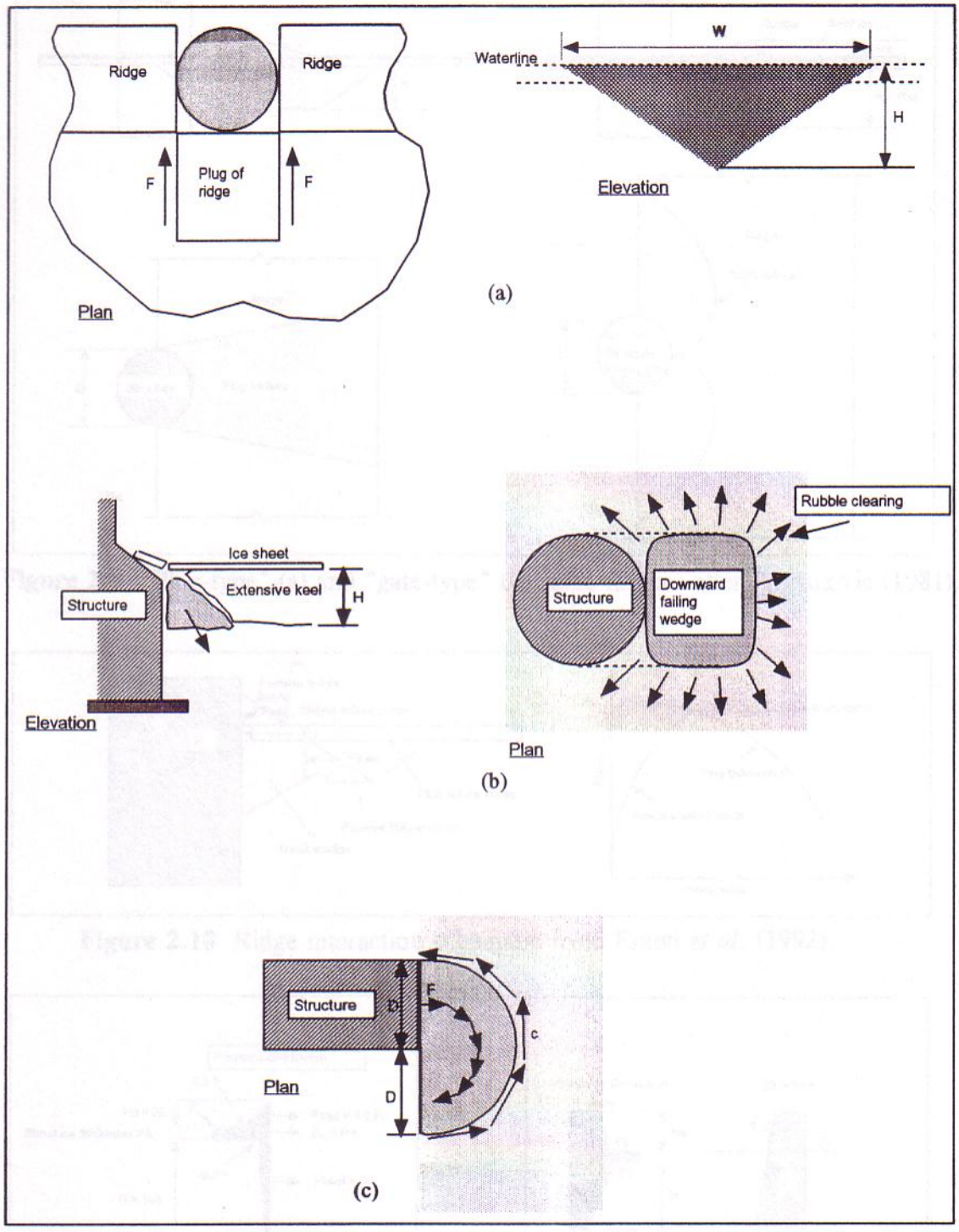

Figure 2.8 First-year ridge keel failure scenarios after Croasdale (1980, 1994). (a) Shear plug (b) wedge and (c) "footing type" failures.

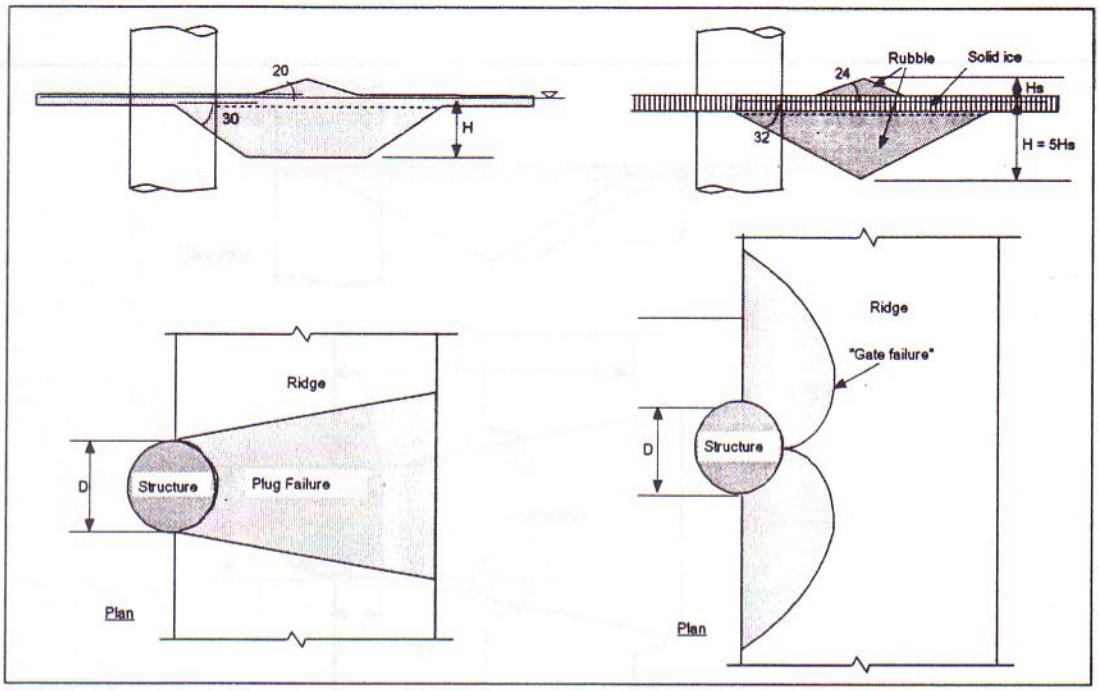

Figure 2.9 "Plug-type" (a) and "gate-type" (b) ridge failures after Prodanovic (1981).

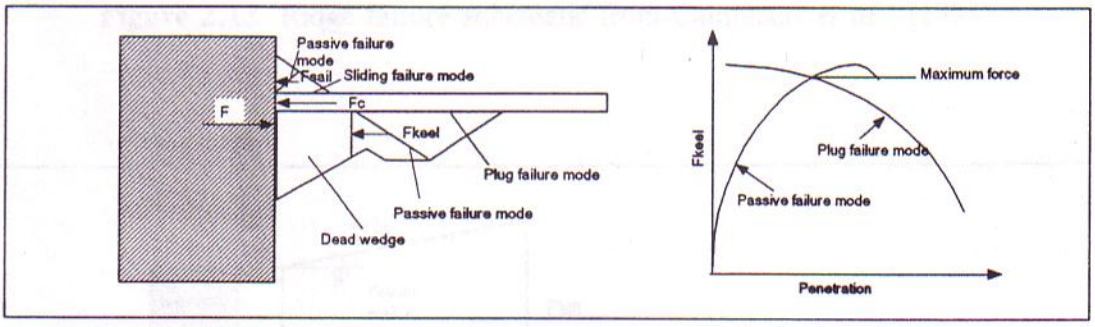

Figure 2.10 Ridge interaction schematic from Eranti *et al.* (1992).

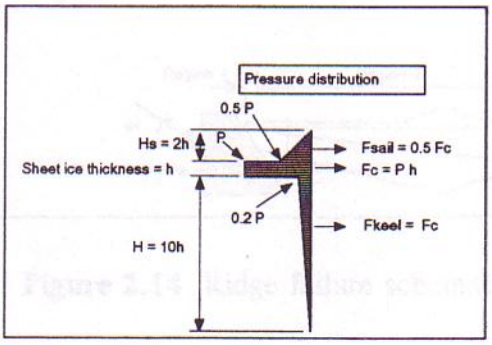

Figure 2.11
Maattanen's ridge pressure (cit. Krankkala and Maattanen, 1984).

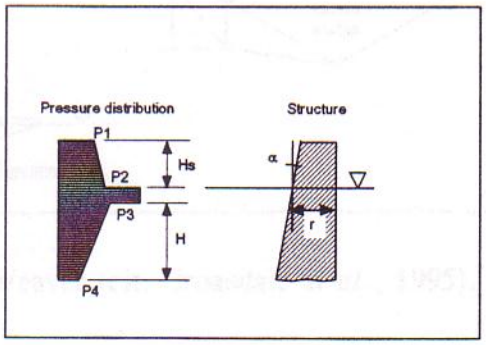

Figure 2.12
Hoikkanen's ridge pressure (cit. Krankkala and Maattanen, 1984).

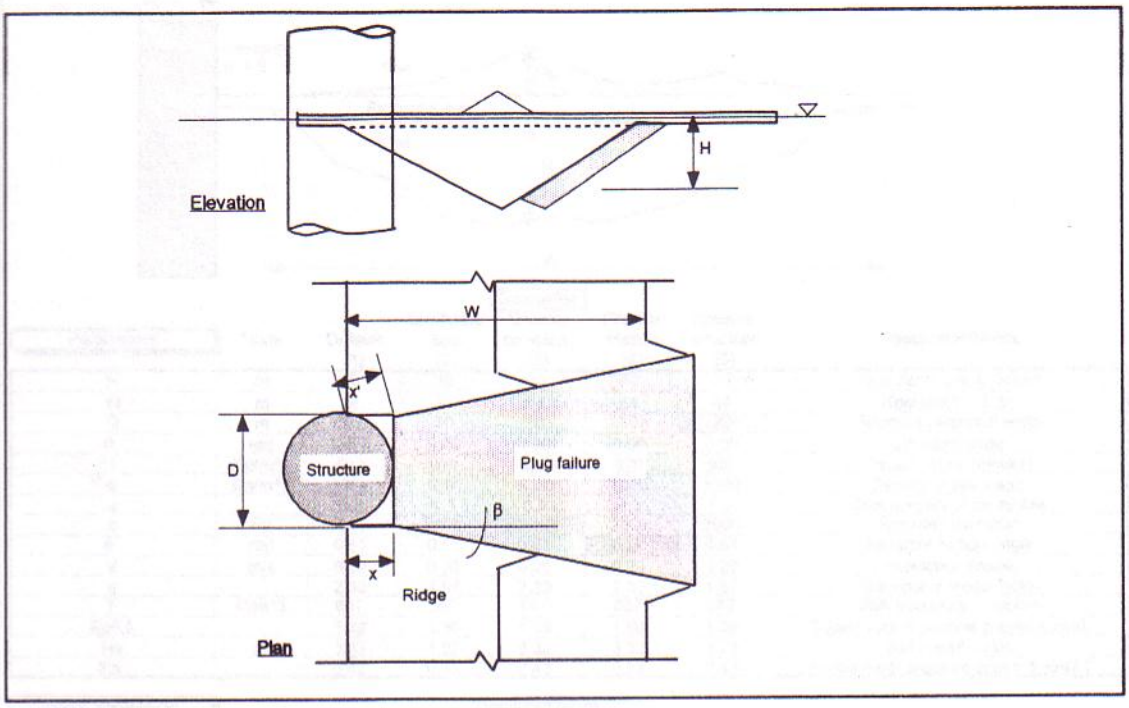

Figure 2.13 Ridge failure schematic from Cammaert *et al.*, (1993).

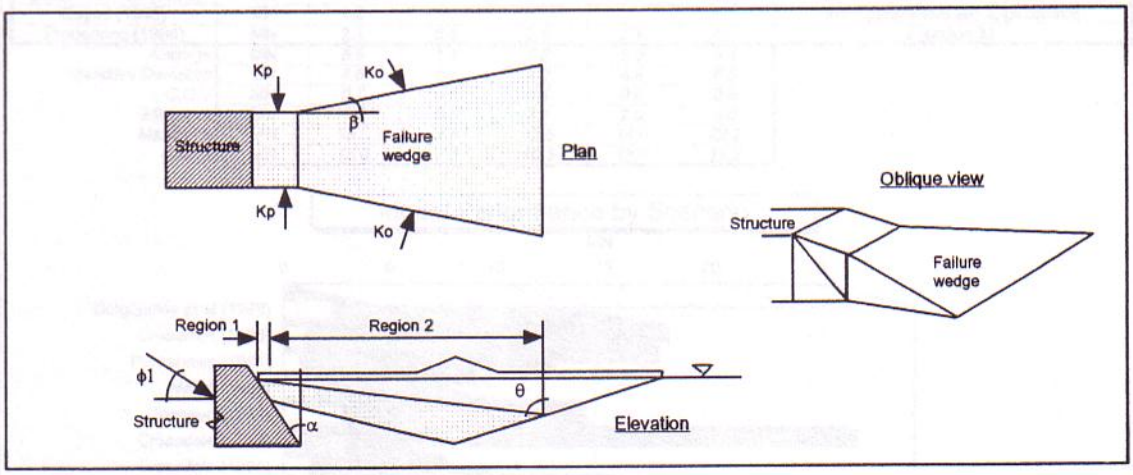

Figure 2.14 Ridge failure schematic from Weaver (cit. Croasdale *et al.*, 1995).

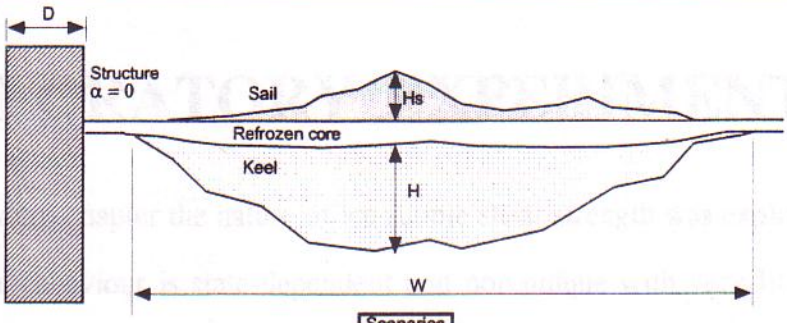

Parameters	Units	Scenarios: Default (1)	Shallower keel (2)	Greater cohesion (3)	Greater friction (4)	Broader structure (5)	Description/Notes
H	m	20	10	20	20	20	Keel depth below datum
W	m	64	32	64	64	64	Keel width = 3.2H
D	m	10	10	10	10	20	Structure projected width
α	rad	0.00	0.00	0.00	0.00	0.00	Structure slope
ρi	Kg/m^3	920	920	920	920	920	Density of ice (blocks)
ρw	Kg/m^3	1020	1020	1020	1020	1020	Density of sea water
e		0.3	0.3	0.3	0.3	0.3	Bulk porosity of ice rubble
c	Pa	2500	2500	5000	2500	2500	Apparent cohesion
ϕ	rad	0.61	0.61	0.61	0.87	0.61	Apparent friction angle
V	m/s	0.20	0.20	0.20	0.20	0.20	Interaction speed
q		2.33	1.67	2.33	2.33	1.67	Dolgopolov shape factor
γ	N/m^3	687	687	687	687	687	Bulk buoyancy of rubble
Kp^.5		1.39	1.39	1.39	1.66	1.39	Square root of passive pressure coef.
Hs	m	3.33	1.67	3.33	3.33	3.33	Sail height = H/6
Ko		0.43	0.43	0.43	0.23	0.43	At-rest earth pressure coef = 1-sin(ϕ)

Model References		Predicted loads					
Dolgopolov et al (1975)	MN	9.4	2.3	12.6	12.7	13.4	Equation 11 (no surcharge)
Croasdale (1980)	MN	8.2	1.0	8.2	14.0	8.2	Equation 20
Prodanovic (1981)	MN	3.2	0.8	6.4	3.2	3.2	Equation 26
Mellor (1981)	MN	4.8	1.5	6.2	6.5	9.6	Equation 19
Joensuu (1981)	MN	11.1	2.8	11.1	11.1	22.2	Equation 32
Croasdale (1994)	MN	2.0	0.8	4.0	2.0	3.0	Equation 22
Croasdale (1994)	MN	7.2	1.3	7.2	12.2	10.3	Equation 25
Brown & Bruce (1995)	MN	16.0					input parameters are approximate
Sayed (1995)	MN	1.0					input parameters are approximate
Frederking (1994)	MN	2.1	0.5	2.1	2.1	4.2	Equation 33
Average	MN	*6.5*	*1.4*	*7.2*	*8.0*	*9.3*	
Standard Deviation	MN	*4.6*	*0.7*	*3.2*	*4.8*	*6.0*	
C.O.V	MN	*0.7*	*0.5*	*0.4*	*0.6*	*0.6*	
Minimum	MN	*1.0*	*0.5*	*2.1*	*2.0*	*3.0*	
Maximum	MN	*16.0*	*2.8*	*12.6*	*14.0*	*22.2*	
Range	MN	*15.0*	*2.3*	*10.5*	*12.0*	*19.2*	

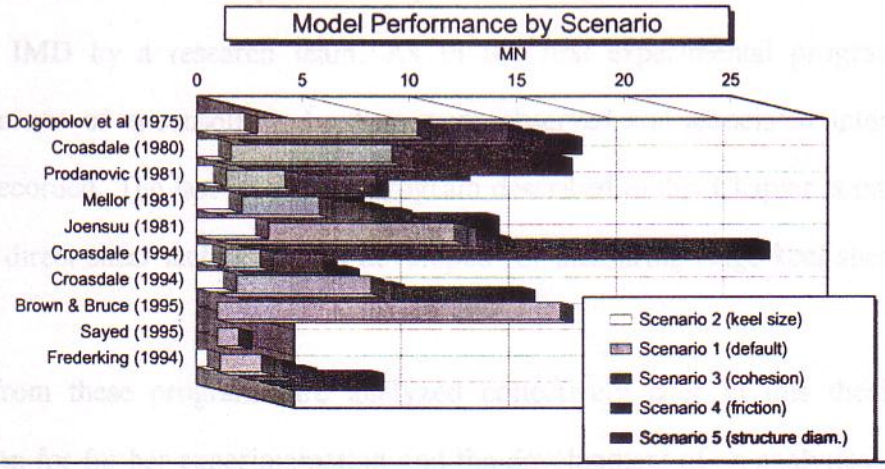

Figure 2.15 Sensitivity study and comparison of ridge keel models.